Electronic Supporting Information

Table of contents

General remarks and material

All solvents were dried using standard procedures; all other reagents were of reagent-grade quality obtained from commercial suppliers and used without further purification. Column chromatography was performed on silica gel 60 (70 – 230 mesh). Melting points were measured with an electrothermal apparatus and are uncorrected. NMR spectra were recorded on a Bruker 400 MHz and an Agilent DD2 500 MHz. Chemical shifts are expressed in ppm (δ) using the residual solvent signal as an internal reference (7.16 ppm for C_6H_6, 7.26 ppm for $CHCl_3$, 3.31 ppm for methanol-d4 and 2.09 ppm for toluene-d8). The terms m, s, d, t, q, and quint represent multiplet, singlet, doublet, triplet, quadruplet, and quintuplet, respectively, and the term br means a broad signal. Calix[6]arene **3** was synthesised according to a published procedure.[1]

Absorption and Luminescence Spectra. UV-vis absorption and luminescence spectra were recorded with a Cary 300 (Agilent) spectrophotometer and an FS5 (Edinburgh) spectrofluorometer, respectively. Measurements were performed on air-equilibrated toluene (Sigma-Aldrich) solutions at room temperature (298 K). All solutions were prepared and examined in a dark room illuminated only by a red light to avoid undesired photoisomerisation of the investigated compounds. Luminescence quantum yields were determined using $[Ru(bpy)_3]Cl_2$ in water (ϕ_f=0.04) as standard. The quantum yields were determined at least on two different samples of the same compound, and the values were averaged. Luminescence lifetimes were measured with an FLS920 (Edinburgh) time-correlated single-photon counting spectrofluorometer, exciting the sample at 405 nm with a pulsed laser.

Characterisation of solid compounds. Solid films of the investigated compounds were prepared by dropcasting dichloromethane solutions (10^{-4} to 10^{-3} M) on quartz slides. The dropcasted solutions were left to dry and then put under a vacuum for 16 h. The obtained films were analysed by transmission UV-Vis spectroscopy. The solid samples meant to be analysed by luminescence spectroscopy were prepared by putting the solid compound between two glass slips or in a quartz tube.

Photochemical characterisation performed by UV-Vis spectroscopy. Irradiation experiments were performed with a Helios Quartz (125 W) and a LOT-QuantumDesign (200 W) medium-pressure mercury lamp in toluene solutions at room temperature (298 K). The photoisomerisation quantum yields of compound **1-Up** were determined, due to a fast thermal return, with a diode array Avantes photometer equipped with an optical fibre and coupled to the LOT-QuantumDesign medium-pressure mercury lamp. This setup allows to record the absorption spectra under continuous irradiation. The desired Hg emission line was selected with

an interference filter. The incident light intensity was measured for each experiment using the dimethylazobenzene actinometer,[2] and it was of the order of 10^{-9} ein/s. The solutions were carefully stirred throughout the whole irradiation to ensure the homogeneity of the solution. The photoisomerisation quantum yields were determined by fitting the time-dependent absorption changes with the model for a T-type photochrome[3] using Berkeley-Madonna.[4] The quantum yields were determined at least on two different samples of the same compound and the values were averaged. Thermal back isomerisation kinetics measurements were performed on previously irradiated solutions kept in the dark by monitoring the absorbance variations over time at room temperature (298 K).

Photochemical characterisation performed by ^{1}H NMR Spectroscopy. Photochemical processes were performed in toluene-d_8 solutions at room temperature (298 K). Irradiation of NMR samples at λ_{irr} ~ 365 nm within the spectrometer probe was performed with a setup adapted from the one described by Gschwind and coworkers.[5] The irradiation system consists of a Prizmatix UHP-T-365-SR LED Illuminator (1.5 W, λ_{max}= 369 nm, FWHM=15.56 nm) equipped with FCA-SMA adaptor for the optical fibre. Irradiation of NMR samples at λ_{irr} ~ 460 nm within the spectrometer probe was performed with a homemade setup of an LZ1-00B202 LED ELGIN LED illuminator (3.3 W, λ_{max}= 457 nm, FWHM=15 nm), equipped with FCA-SMA adaptor for the optical fibre. Quartz optical fibre (core 1000 µm, 5 m) with an SMA connector on one end was purchased from Thorlabs; the other end of the optical fibre was scraped to remove the protective coating and was submerged into the solution within the NMR tube to be irradiated.

X-ray crystallographic characterisation. Single crystal XRD measurement on **1-Down** was performed at low temperature (200K) with a Bruker Venture D8 diffractometer equipped with Photon II area detector, using a CuKα microfocus radiation source (λ = 1.54184). The data collection strategy comprised a series of phi and omega scans. Data were indexed, integrated, and scaled using CrysAlis Pro software.[6] The structures were solved by the dual space algorithm implemented in the SHELXT code[7] in Olex2.[8] Fourier analysis and refinement were performed by the full-matrix least-squares methods based on F2 implemented in SHELXL-2014.[9]

Synthesis

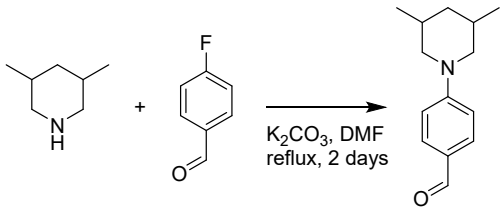

5

Synthesis of 4-(3,5-dimethylpiperidin-1-yl)benzaldehyde (5).[10] In a double-necked round-bottomed flask, 3,5-dimethylpyridine (0.46 g, 4.03 mmol) and 4-fluorobenzaldehyde (0.5 g, 4.03 mmol) were dissolved in 40 ml of dry DMF under inert atmosphere. Potassium carbonate (1.67 g, 12.1 mmol) was added, and the reaction mixture was refluxed for two days. After completion of the reaction, the mixture was poured into ice water. The precipitated product was filtered and then purified by column chromatography on silica gel (*n*-Hex/EtOAc 8:2) to yield 0.62 g of **5** (68%) as a yellow oil. The spectral data are in agreement with those previously reported.[10] ^{1}H NMR (400 MHz, $CDCl_3$): δ (ppm) = 9.73 (s, 1H), 7.71 (d, 2H, *J* = 7.7 Hz), 6.88 (d, 2H, *J* = 6.9 Hz), 3.86 (m, 2H), 2.41 (dd, 2H, *J* = 12.9, 11.3 Hz), 1.85 (m, 1H), 1.71 (m, 2H), 0.94 (d, 6H, *J* = 6.6 Hz), 0.80 (m, 1H). For a complete protons assignment, see Fig. S1.

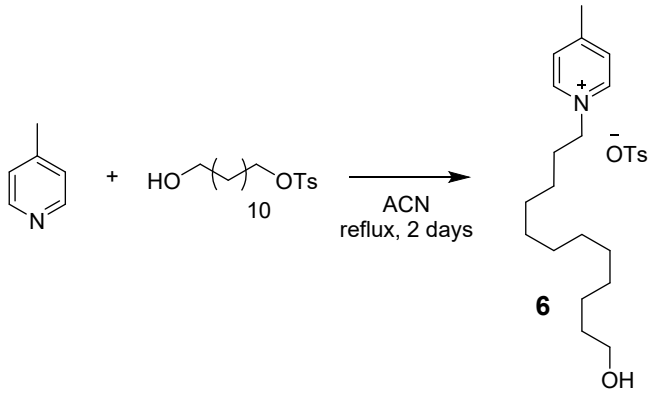

Synthesis of 1-(12-hydroxydodecyl)-4-methylpyridin-1-ium tosylate (6). In a two-necked round-bottomed flask, picoline (95 mg, 1.02 mmol) and 1,12-dodecanediol monotosylate (0.4 g, 1.12 mmol) were dissolved in about 20 ml of dry acetonitrile under inert atmosphere. The reaction mixture was refluxed for two days. Afterwards, the solution was evaporated to dryness under reduced pressure. The solid residue was recrystallised from ethyl acetate to afford 0.37 g of **6** as a white solid (81%). M. p.= 100 − 102 °C. ^{1}H NMR (400 MHz, methanol-d_4): δ (ppm) = 8.78 (d, 2H, *J* = 6.3 Hz), 7.90 (d, 2H, *J* = 6.3 Hz), 7.70 (d, 2H, *J* = 6 Hz), 7.23 (d, 2H, *J* = 6 Hz), 4.53 (t, 2H, *J* = 6.6 Hz), 3.54 (t, 2H, *J* = 6.64 Hz), 2.66 (s, 3H), 2.37 (s, 3H), 1.99 (m, 2H), 1.53 (m, 2H), 1.40-1.26 (m, 16H). ^{13}C NMR (100 MHz, methanol-d_4): δ = 159.78, 143.43, 142.30, 140.24, 128.48, 128.44, 125.57, 61.59, 60.79, 32.27, 30.97, 29.34, 29.26, 29.21, 29.10, 28.71, 25.76, 25.56, 20.55, 19.94. ESI-MS: *m/z* [M-OTs]$^{+}$ calcd. for $C_{18}H_{32}NO$: 278.25; found: 278.41. For a complete protons assignment, see Fig. S2.

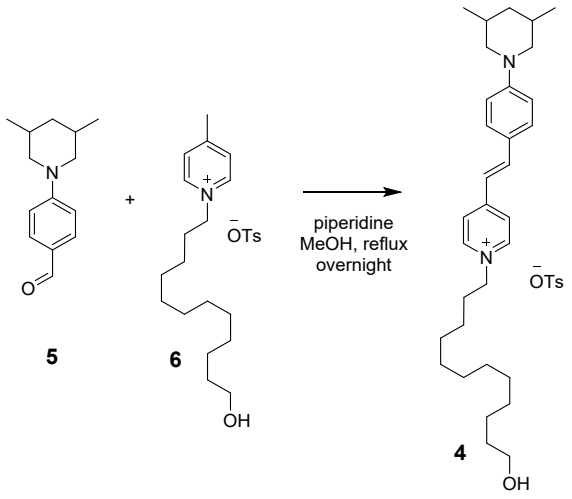

Synthesis of (*E*)-4-(4-(3,5-dimethylpiperidin-1-yl)styryl)-1-(12-hydroxydodecyl)pyridin-1-ium tosylate (4). In a two-necked round-bottomed flask, **5** (0.12 g, 0.546 mmol) and **6** (0.21 g, 0.455 mmol) were dissolved in about 10 ml of methanol under an inert atmosphere. Then, piperidine (58 mg, 0.683 mmol) was added, and the reaction mixture was refluxed overnight. Afterwards, the solution was evaporated to dryness under reduced pressure, and the solid residue was recrystallised from ethyl acetate to afford 0.25 g of **4** as a red solid (86%). M. p. = 151 - 153°C. ^{1}H NMR (400 MHz, $CDCl_3$): δ (ppm) = 8.74 (d, 2H, *J* = 6.5 Hz), 7.83 (d, 4H, *J* = 8.2 Hz), 77.51 (d, 1H, *J* = 16 Hz), 7.45 (d, 2H, *J* = 8.7 Hz), 7.13 (d, 2H, *J* = 8 Hz), 6.88 (d, 2H, *J* = 8.3 Hz), 6.78 (d, 1H, *J* = 16 Hz), 4.40 (t, 2H, *J* = 7.4 Hz), 3.75 (d, 2H, *J* = 11.0), 3.59 (t, 2H, *J* = 6.7), 2.37 (t, 2H, *J* = 12 Hz), 2.31 (s, 3H), 1.90 - 1.70 (m, 3H), 1.52 (m, 2H), 1.36 – 1.12 (m, 18H), 0.93 (d, 6H, *J* = 6.5 Hz), 0.78 (q, 1H, *J* = 12 Hz). ^{13}C NMR (100 MHz, $CDCl_3$): δ = 153.82, 144.07, 143.81, 142.27, 139.27, 130.59, 128.75, 126.15, 123.28, 117.76, 114.94, 62.82, 60.47, 55.64, 42.16, 32.88, 31.57, 30.63, 29.48, 29.39, 29.34, 29.28, 29.00, 26.09, 25.81, 21.45,

19.37. ESI-MS: *m/z* [M-OTs]$^+$ calcd. for $C_{32}H_{49}N_2O$: 477.38; found: 477.48. For a complete protons assignment, see Fig. S4.

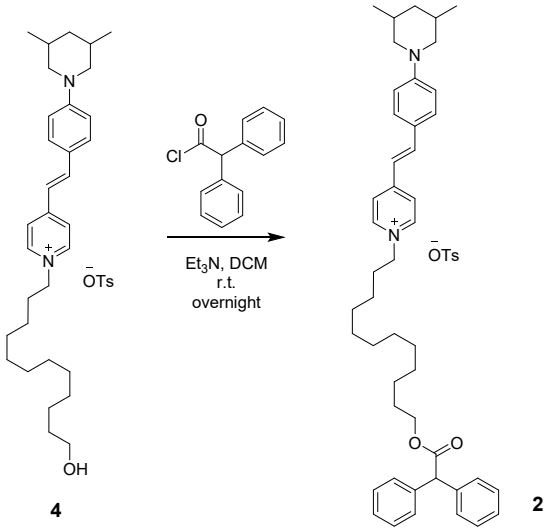

Synthesis of (*E*)-4-(4-(3,5-dimethylpiperidin-1-yl)styryl)-1-(12-(2,2-diphenylacetoxy)dodecyl)pyridin-1-ium tosylate (2). Triethylamine (9.5 µL, 68 µmol) was added to a mixture of **4** (40 mg, 62 µmol) and diphenylacetyl chloride (16 mg, 68 µmol) in dry dichloromethane (2 mL, 0.03 M) under nitrogen at room temperature. The mixture was stirred at room temperature overnight. The mixture was concentrated under vacuum, and the crude residue was purified by flash column chromatography on silica gel (dichloromethane/methanol 9:1) to afford **2** (45 mg, 87%) as a red waxy solid. ^{1}H NMR (400 MHz, methanol-d_4): δ (ppm) = 8.57 (d, 2H, *J* = 6.8 Hz), 7.96 (d, 2H, *J* = 7.0 Hz), 7.97 (d, 1H, *J* = 6 Hz), 7.71 (d, 2H, *J* = 8.2 Hz), 7.59 (d, 2H, *J* = 9.0 Hz), 7.32-7.22 (m, 10H), 7.21 (d, 2H, *J* = 7.9 Hz), 7.09 (d, 1H, *J* = 16.0 Hz), 6.96 (d, 2H, *J* = 9.0 Hz), 5.06 (s, 1H), 4.40 (t, 2H, *J* = 7.4 Hz), 4.12 (t, 2H, *J* = 6.5 Hz), 3.87 (m, 2H), 2.36 (t, 2H, *J* = 7.9 Hz), 2.34 (s, 3H),1.94 (m, 2H), 1.84 (m, 1H), 1.72 (m, 2H), 1.57 (m, 3H), 1.39-1.18 (m, 16H), 0.96 (d, 6H, *J* = 6.6 Hz), 0.80 (q, 1H, *J* = 12.1 Hz). ^{13}C NMR (100 MHz, methanol-d_4): δ =174.3, 156.2, 155.3, 154.3, 144.4, 143.9, 143.7, 141.6, 140.3, 131.6, 129.8, 129.7, 129.5, 128.2, 126.9, 125.5, 123.9, 118.6, 115.7, 71.9, 66.2, 61.3, 58.3, 56.3, 55.4, 43.5, 32.2, 31.8, 30.7, 30.6, 30.5, 30.5, 30.4, 30.1, 30.1, 29.6, 28.7, 27.3, 27.1, 26.9, 21.3, 19.5, 19.0. ESI-MS: *m/z* [M-OTs]$^+$ calcd. for $C_{46}H_{59}N_2O_2$: 671.45; found: 671.33. For a complete proton assignment, see Fig. S6.

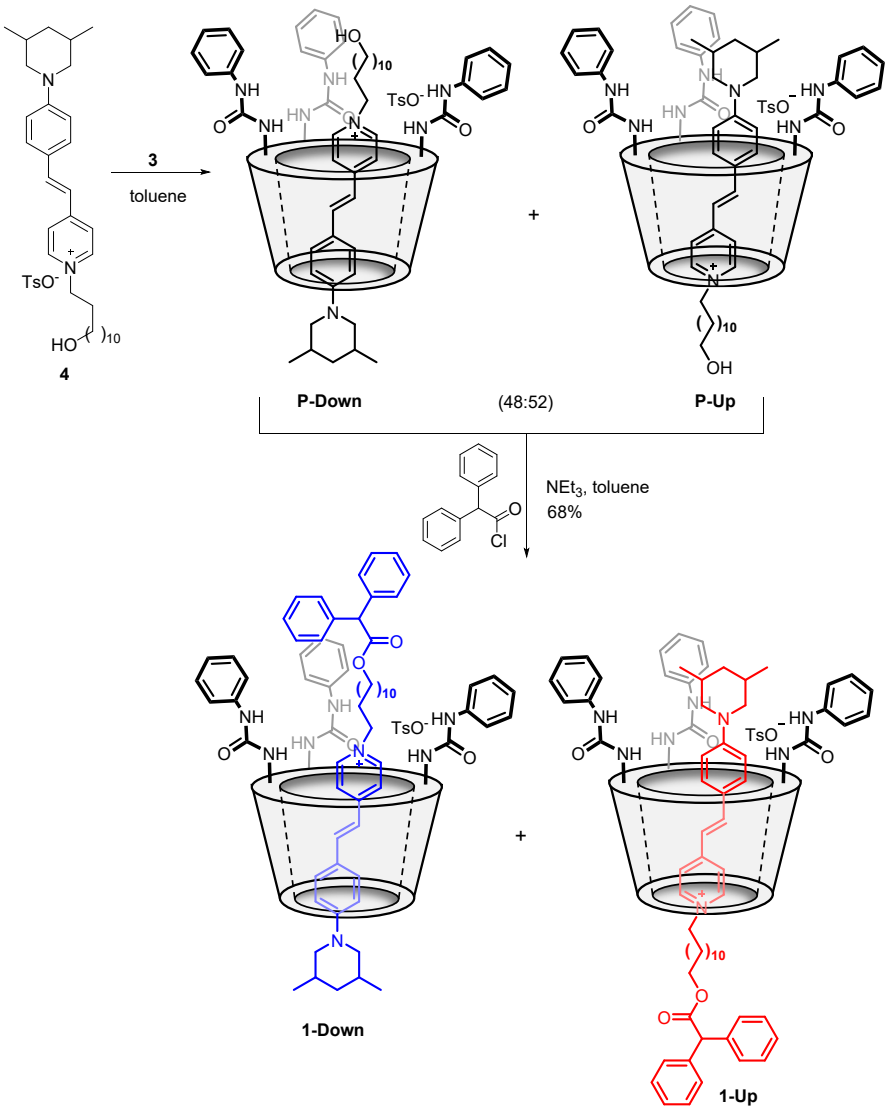

Synthesis of the orientational rotaxane isomers 1-Up and 1-Down. In a two-necked round-bottomed flask, **4** (80 mg, 0.123 mmol) and **3** (0.234 g, 0.160 mmol) were dissolved in about 1.5 ml of dry toluene and left equilibrating under magnetic stirring for 2 hours at room temperature. Afterwards, diphenyl acetyl chloride (31.2 mg, 0.135 mmol) and triethylamine (19 µL, 0.135 mmol) were added to the solution, and the reaction mixture was stirred at room temperature overnight. After this period, the solvent was evaporated under reduced pressure. The solid residue was purified by column chromatography on silica gel (*n*-Hex/EtOAc = 7:3) to yield a mixture of the two orientational isomers, with an overall yield of 68%. Next, the two isomers were separated through plate chromatography (dichloromethane/methanol= 96:4) to afford 0.132 g of **1-Up**, as an orange solid (31%), and 0.163 g of **1-Down**, as a yellow solid (37%).

1-Up: M. p. = 134 – 136 °C. ^{1}H NMR (400 MHz, benzene-d_6): δ (ppm) = 8.20 (d, 2H, *J* = 7.6 Hz), 7.66 – 7.48 (bs, 4H), 7.40 (d, 2H, *J* = 7.2 Hz), 7.31 (bs, 1H), 7.12 (d, 2H, *J* = 7.64 Hz), 7.05 (d, 2H, *J* = 7.26 Hz), 7.02 (bs, 1H), 6.97 (bs, 2H), 6.35 (d, 2H, *J* = 5.90 Hz), 6.08 (bs, 2H), 5.07 (s, 1H), 4.58 (bs, 6H), 4.05 (t, 2H, *J* = 6.75 Hz), 3.92 (bs, 9H), 3.87 (bs, 6H), 3.63 (bs, 6H), 3.43 (q, 6H, *J* = 7 Hz), 3.32 (m, 2H), 1.98 (s, 3H), 1.89 (t, 2H, *J* = 11.8 Hz), 1.55 (bs, 30H), 1.46 (m, 2H), 1.41 (m, 2H), 1.16 (bs, 13H), 0.79 (d. 6H, *J* = 6.40 Hz), 0.46 (q, 1H, *J* = 12.4 HZ). ^{13}C NMR (100 MHz, benzene-d_6): δ = 172.29, 154.43, 153.17, 151.90, 149.09, 147.72, 143.72, 140.60, 139.55, 136.89, 133.84, 132.78, 130.40, 129.33, 129.08, 128.87, 128.74, 127.49, 126.89, 124.86, 121.99, 121.48, 119.14, 118.65, 114.70, 72.70, 70.48, 66.70, 65.09, 61.16, 57.70, 55.47, 42.48, 34.73, 31.92, 31.24, 30.94, 30.56, 30.41, 30.11, 29.73, 29.64, 28.95, 26.18, 21.17, 19.49, 15.59. HR-MS (ESI, Orbitrap LQ) calculated for

$C_{136}H_{167}N_8O_{14}$ [M-OTs]: m/z (z = 1): 2136.25963, 2137.26298, 2138.26634, 2139.26969, 2140.27305; found: 2136.26099, 2137.26416, 2138.26733, 2139.27026, 2140.27271; calculated for $C_{136}H_{168}N_8O_{14}$ [M-OTs+H]: m/z (z = 2): 1068.63345, 1069.13513, 1069.63681, 1070.13848, 1070.64016; found: 1068.63391, 1069.13538, 1069.63672, 1070.13831, 1070.64014. For a complete protons assignment, see Fig. S10.

1-Down: M. p. = 143 – 145 °C. ^{1}H NMR (400 MHz, benzene-d_6): δ (ppm) = 8.15 (d, 2H, *J* = 7.9 Hz), 8.07 (bs, 2H), 7.82 – 7.6 (bs, 6H), 7.58 (bs, 4H), 7.43 (d, 2H, *J* = 7.6 Hz), 7.19 – 6.93 (bs, 10H), 6.90 – 6.74 (bs, 6H), 6.49 (bs, 2H), 6.14 (bs, 2H), 5.11 (s, 1H), 4.59 (bs, 6H), 4.10 (t, 2H, *J* = 6.75 Hz), 3.91 (bs, 9H), 3.63 (bs, 12H), 3.40 (bs, 8H), 2.11 (t, 2H, *J* = 12 Hz), 1.97 (s, 3H), 1.72 - 1.34 (bs, 30H), 1.38 – 1.15 (bs, 6H), 1.10 (t, 2H, *J* = 6.96), 1.05 – 0.78 (bs, 10H), 0.74 (d, 6H, *J* = 6.40 Hz), 0.44 (q, 1H, *J* = 12.4 HZ). ^{13}C NMR (100 MHz, benzene-d_6): δ = 172.37, 154.90, 153.48, 152.34, 149.87, 147.32, 143.23, 140.51, 140.07, 139.69, 139.27, 136.32, 134.47, 132.84, 130.34, 129.15, 129.09, 128.86, 127.43, 126.80, 123.34, 122.25, 119.15, 118.27, 155.55, 73.41, 70.56, 66.74, 65.44, 61.86, 57.75, 56.26, 42.24, 34.68, 31.99, 30.89, 30.40, 30.22, 29.90, 29.64, 29.08, 26.34, 23.17, 21.16, 19.32, 15.56, 14.38. HR-MS (ESI, Orbitrap LQ) calculated for $C_{136}H_{167}N_8O_{14}$ [M-OTs]: m/z (z = 1): 2136.25963, 2137.26298, 2138.26634, 2139.26969, 2140.27305; found: 2136.26074, 2137.26392, 2138.26733, 2139.27026, 2140.27319; calculated for $C_{136}H_{168}N_8O_{14}$ [M-OTs+H]: m/z (z = 2): 1068.63345, 1069.13513, 1069.63681, 1070.13848, 1070.64016; found: 1068.63345, 1069.13513, 1069.63681, 1070.13848, 1070.64016. For a complete protons assignment, see Fig. S18.

NMR and MS characterisation

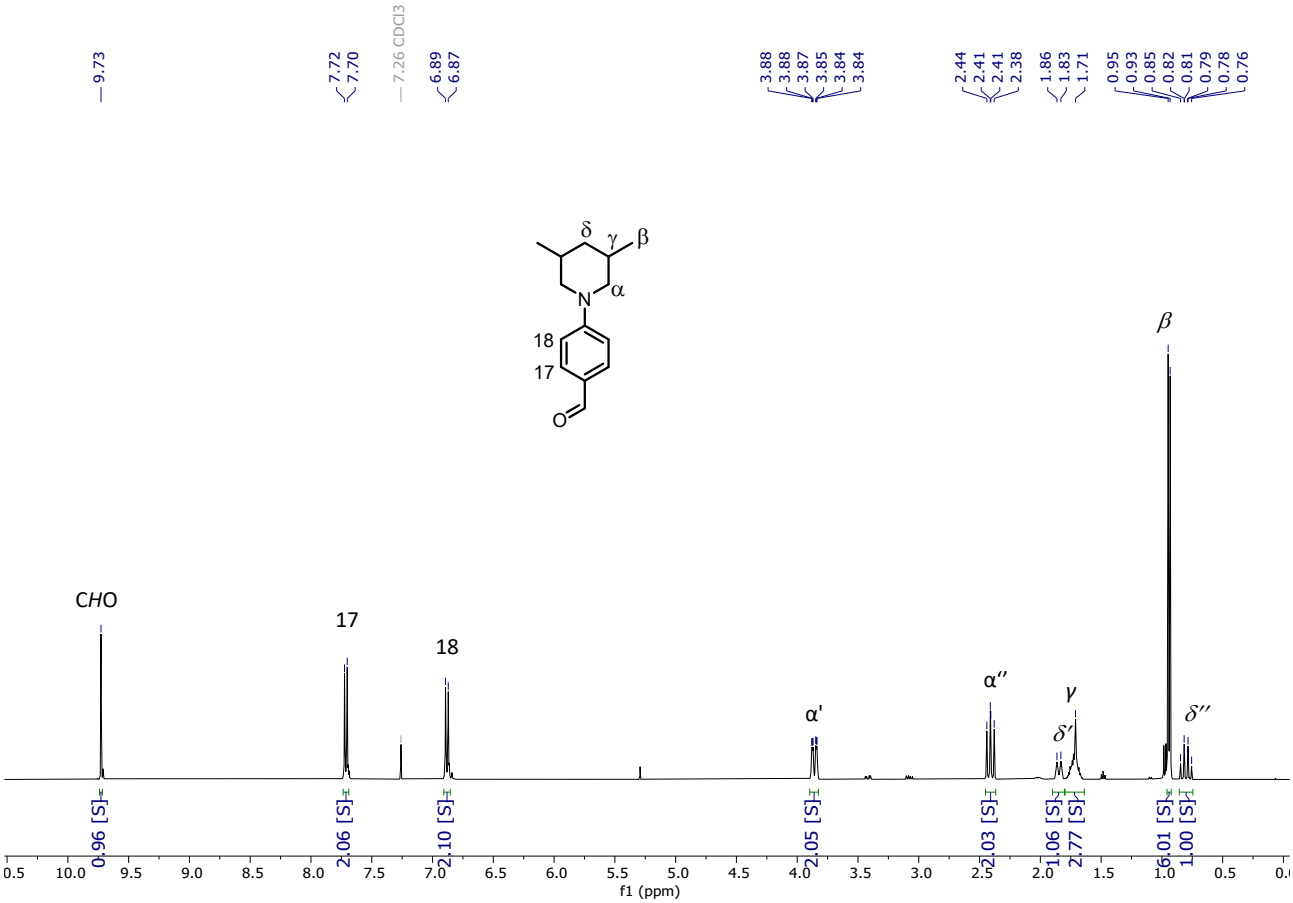

Figure S1: ^{1}H NMR spectrum of compound **5** (400 MHz, $CDCl_3$, 25 °C).

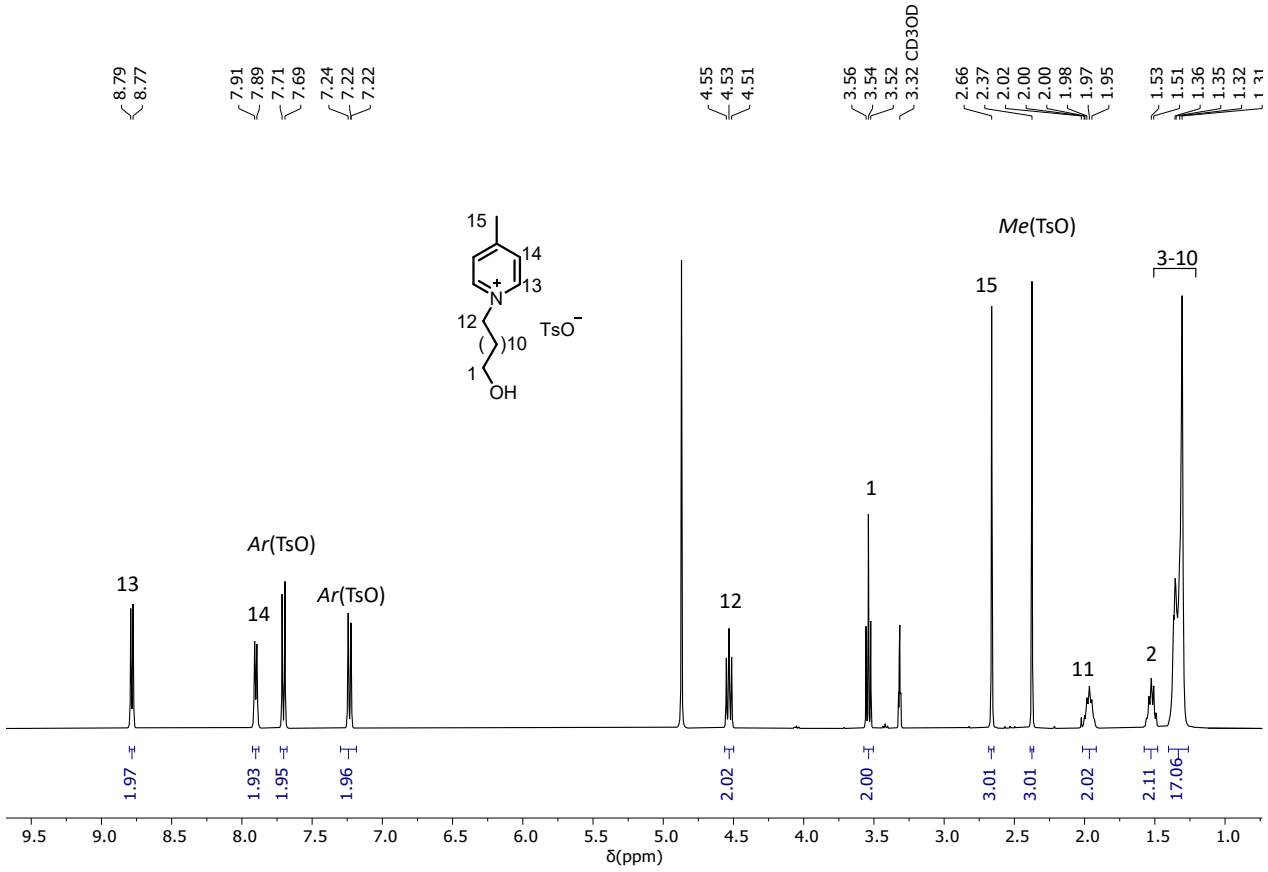

Figure S2: ^{1}H NMR spectrum of compound **6** (100 MHz, CD_3OD, 25 °C).

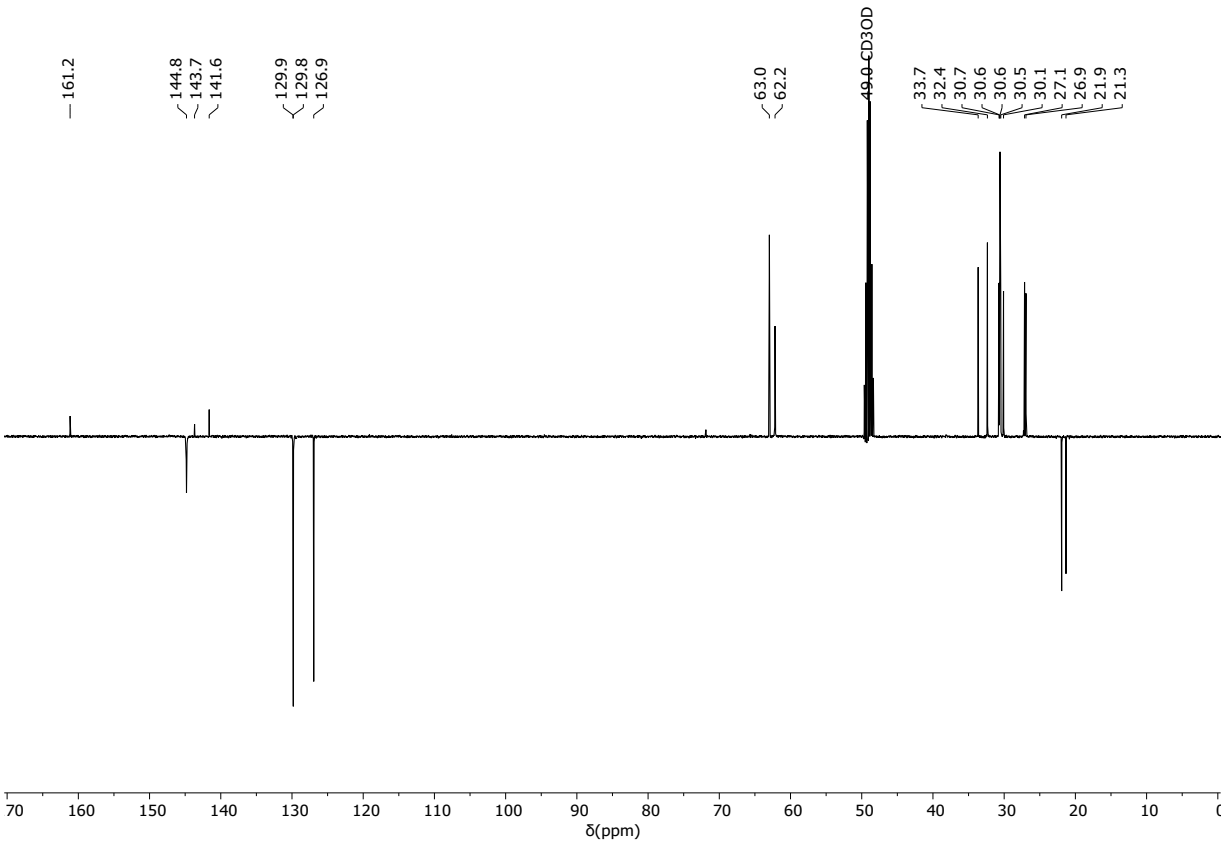

Figure S3: ^{13}C-APT NMR spectrum of compound **6** (100 MHz, CD_3OD, 25 °C).

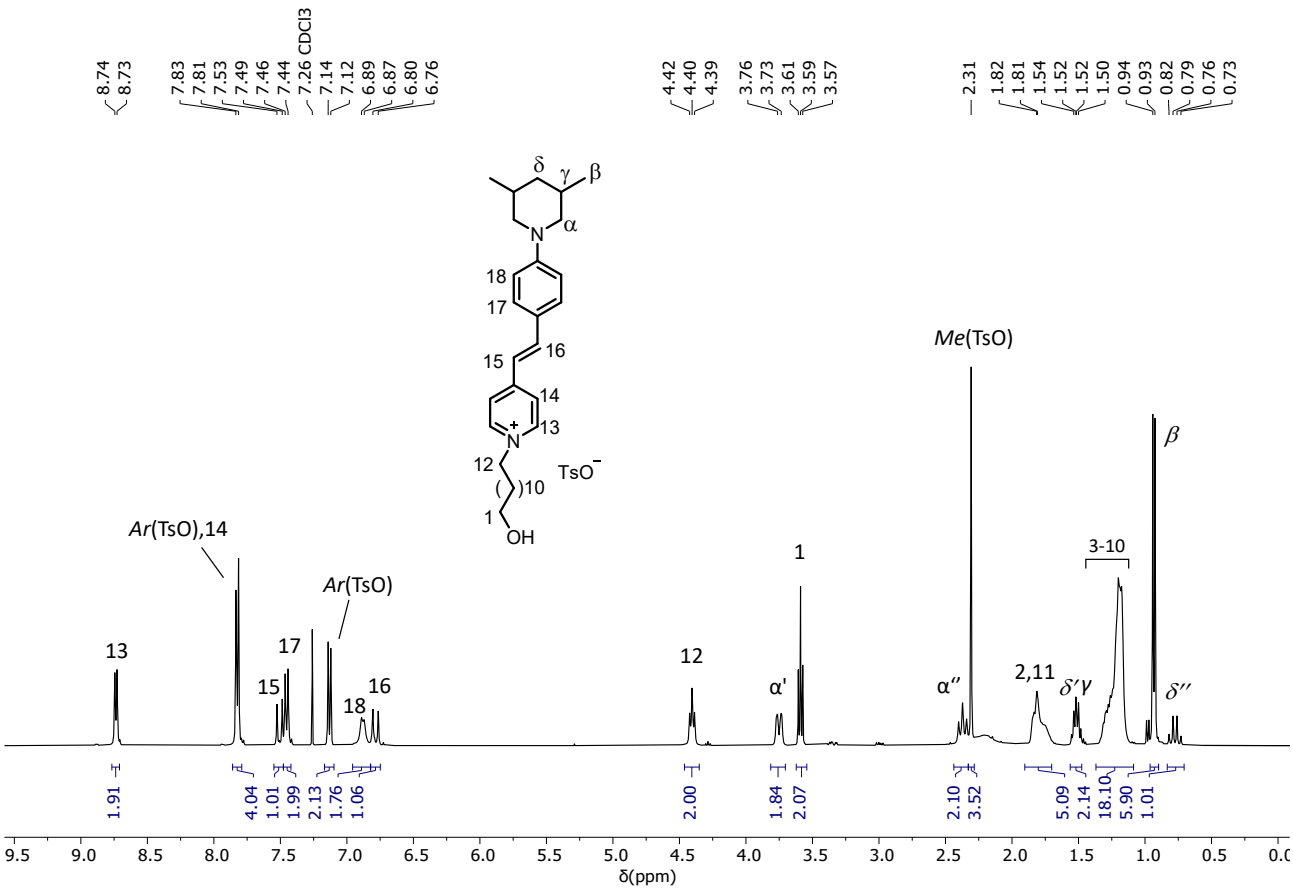

Figure S4: ^{1}H NMR spectrum of compound **4** (400 MHz, $CDCl_3$, 25 °C).

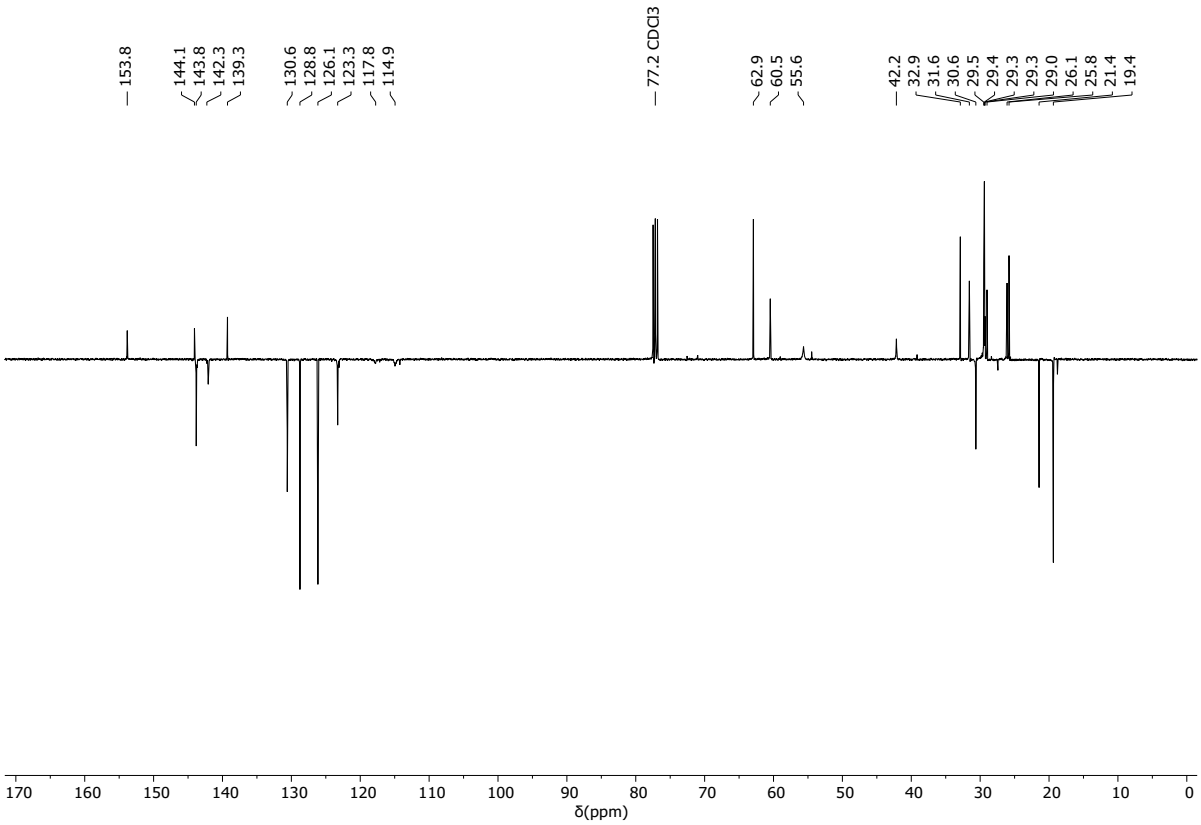

Figure S5: ^{13}C-APT NMR spectrum of compound **4** (100 MHz, $CDCl_3$, 25 °C).

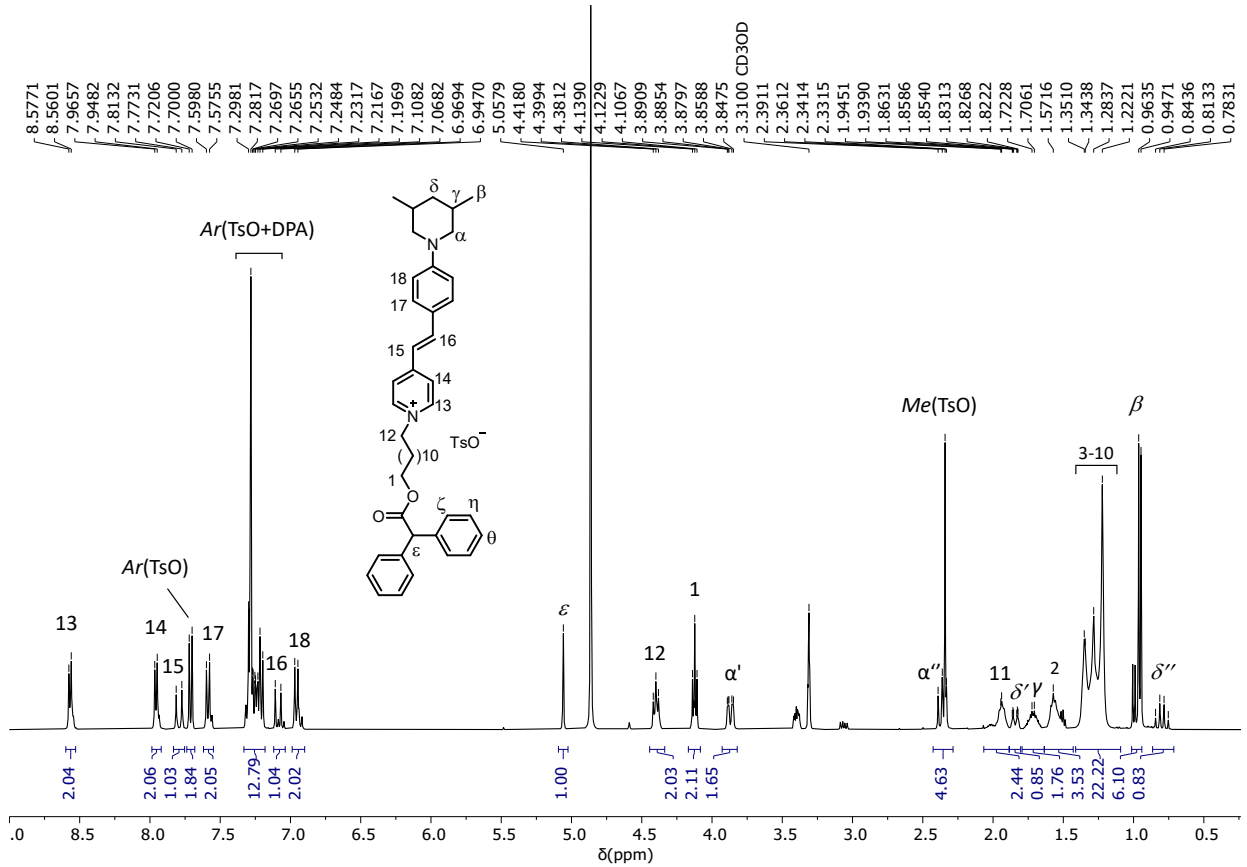

Figure S6: ^{1}H NMR spectrum of compound **2** (400 MHz, CD_3OD, 25 °C).

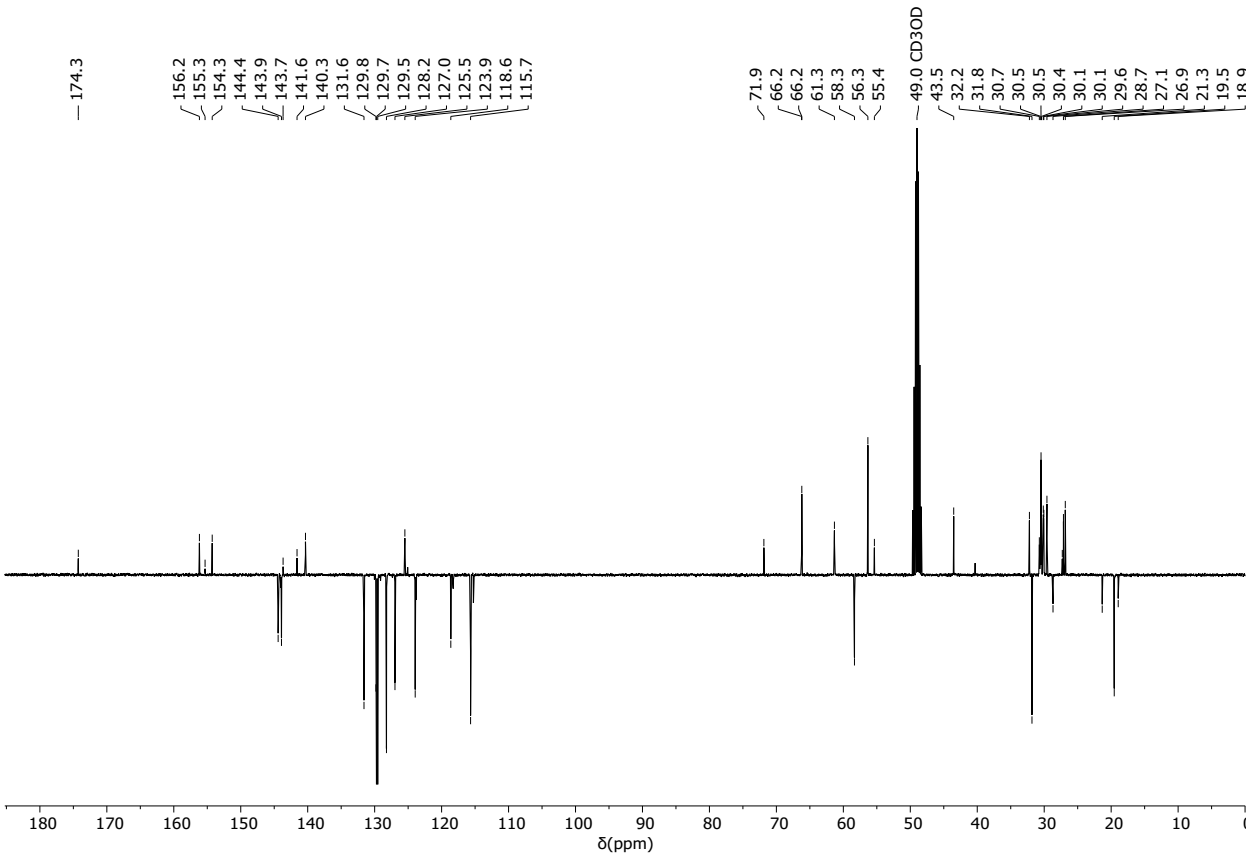

Figure S7: ^{13}C-APT NMR spectrum of compound **2** (100 MHz, CD_3OD, 25 °C).

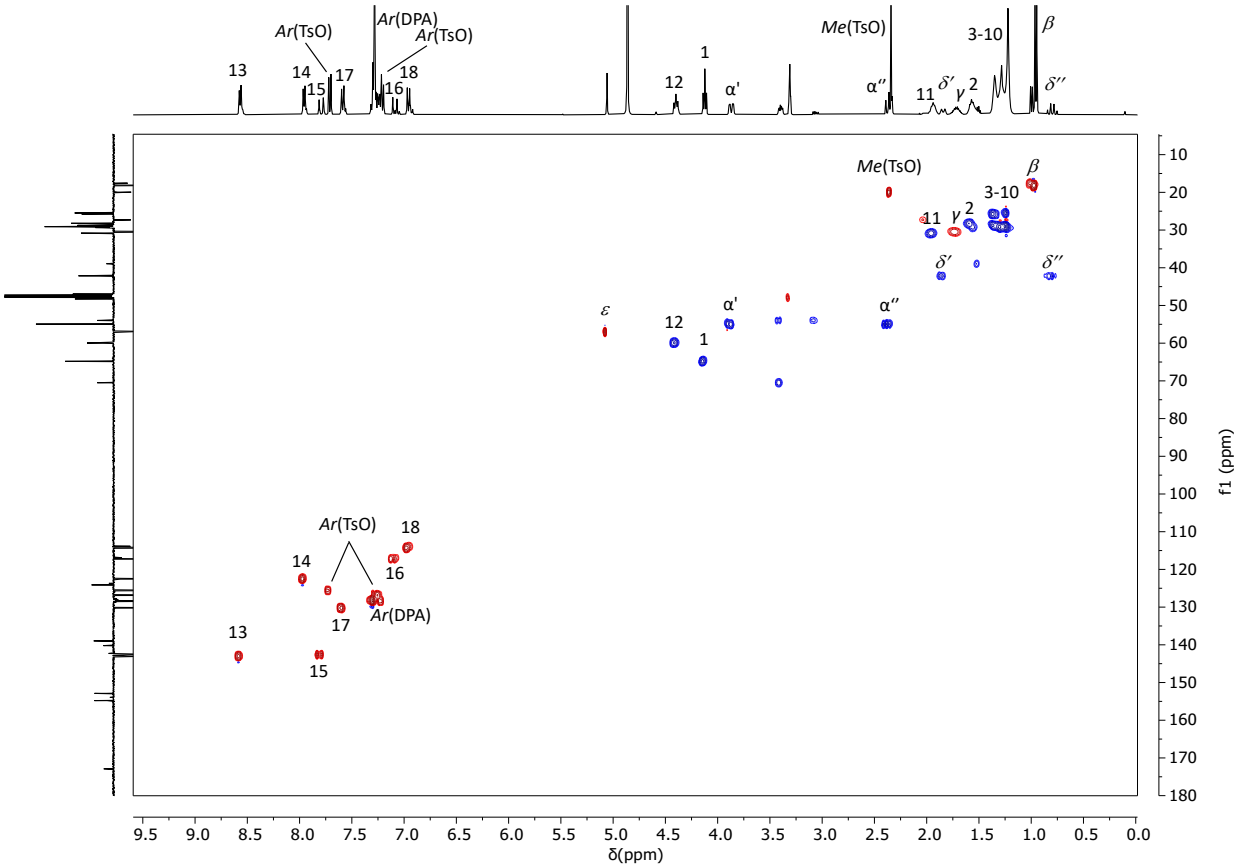

Figure S8: 2D edited-HSQC NMR spectrum of compound **2** (400 MHz, CD_3OD, 25 °C). Red contours identify CH correlations in CH_3 and CH groups, while blue ones show those in CH_2 groups.

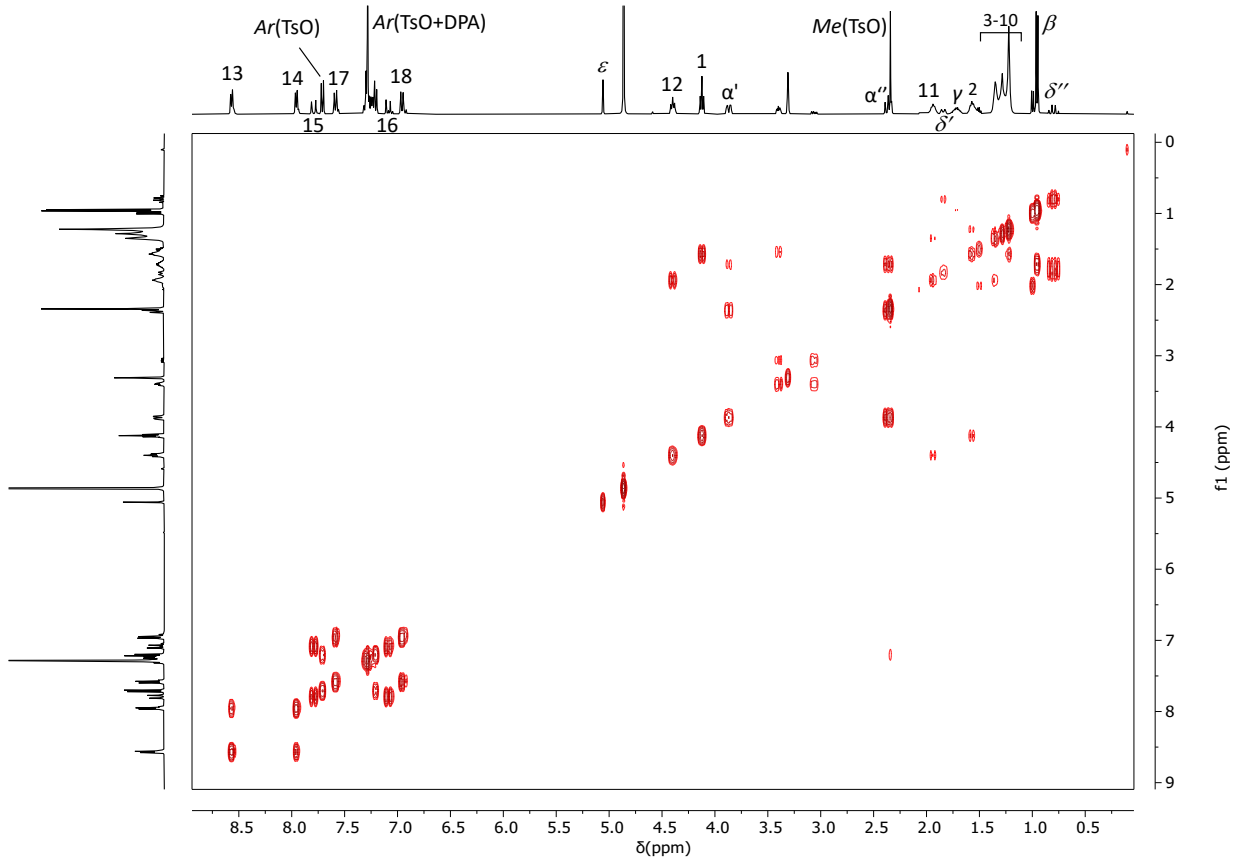

Figure S9: 2D g-COSY NMR spectrum of compound **2** (400 MHz, CD_3OD, 25 °C).

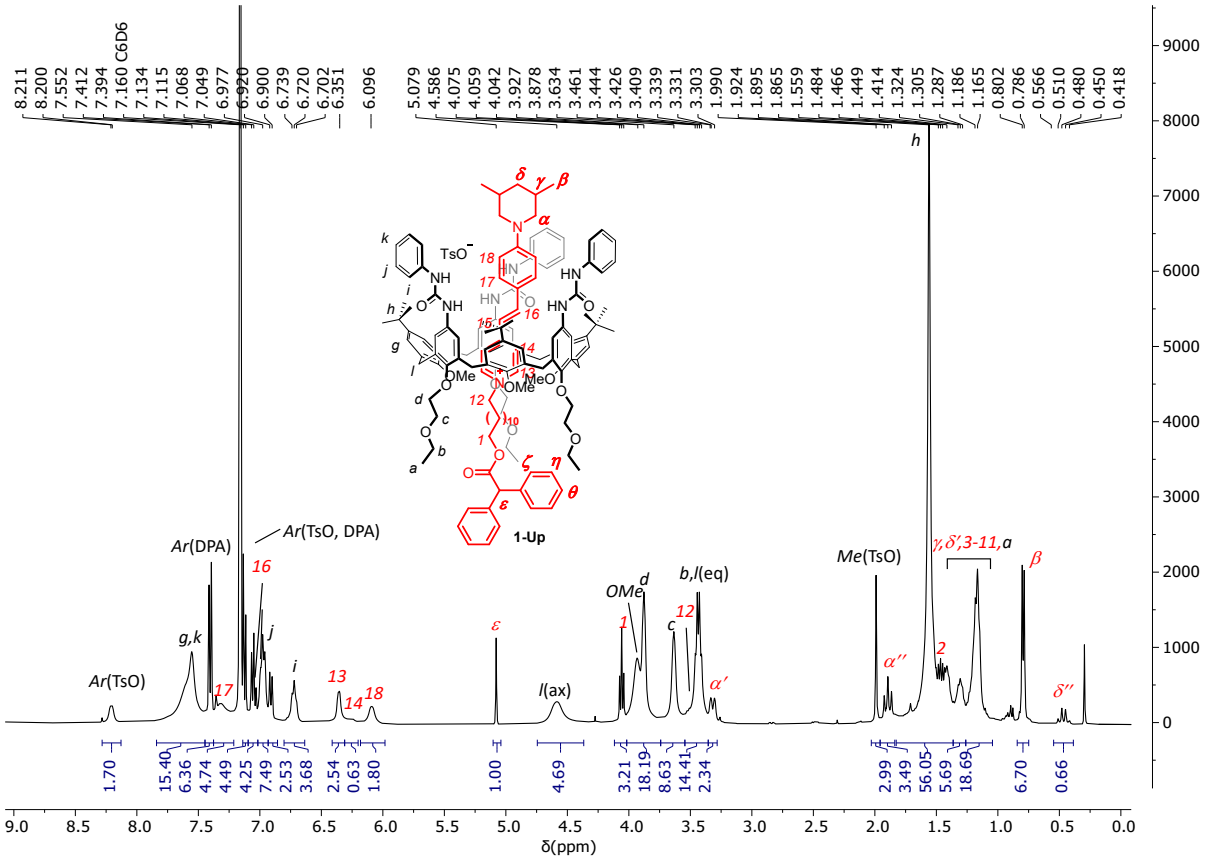

Figure S10: ^{1}H NMR spectrum of compound **1-Up** (400 MHz, C_6D_6, 25 °C).

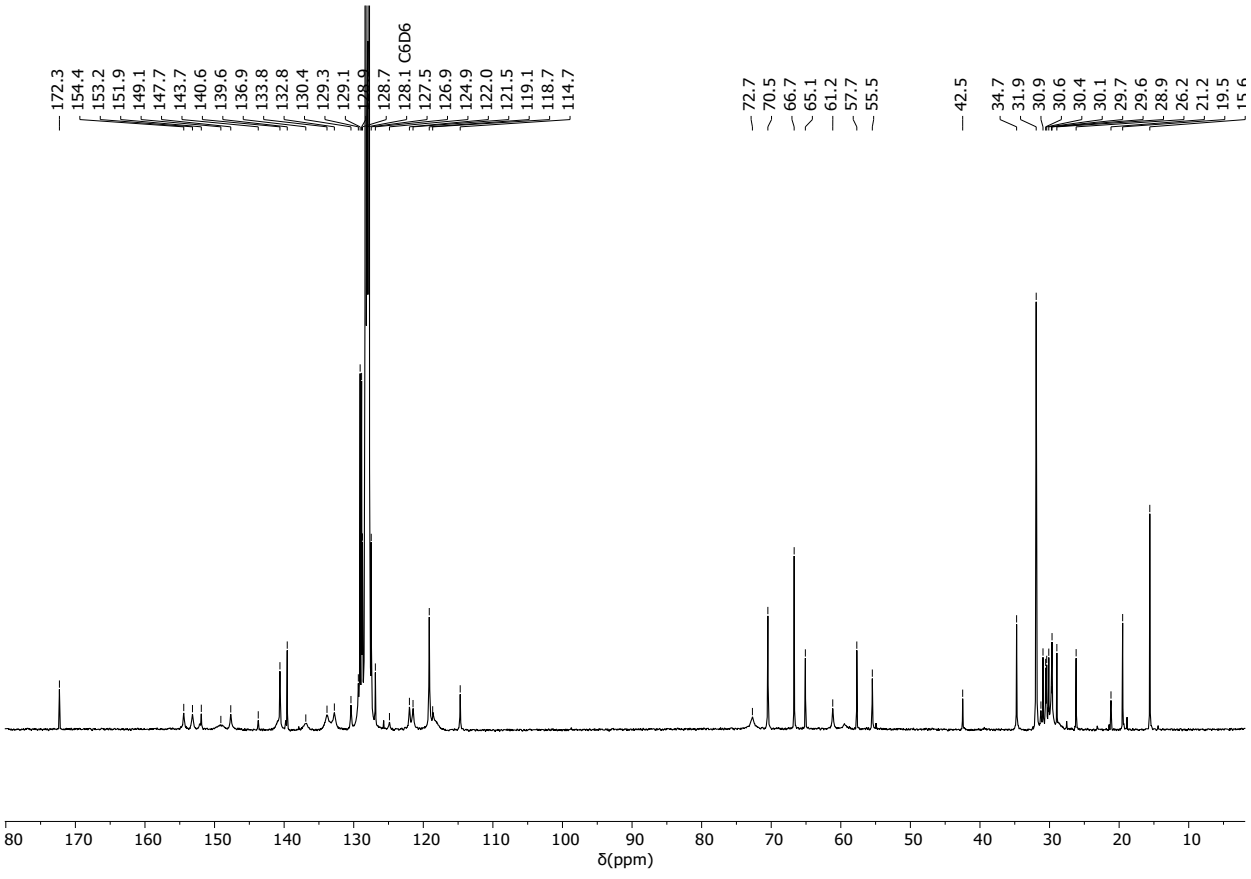

Figure S11: ^{13}C NMR spectrum of compound **1-Up** (100 MHz, C_6D_6, 25 °C).

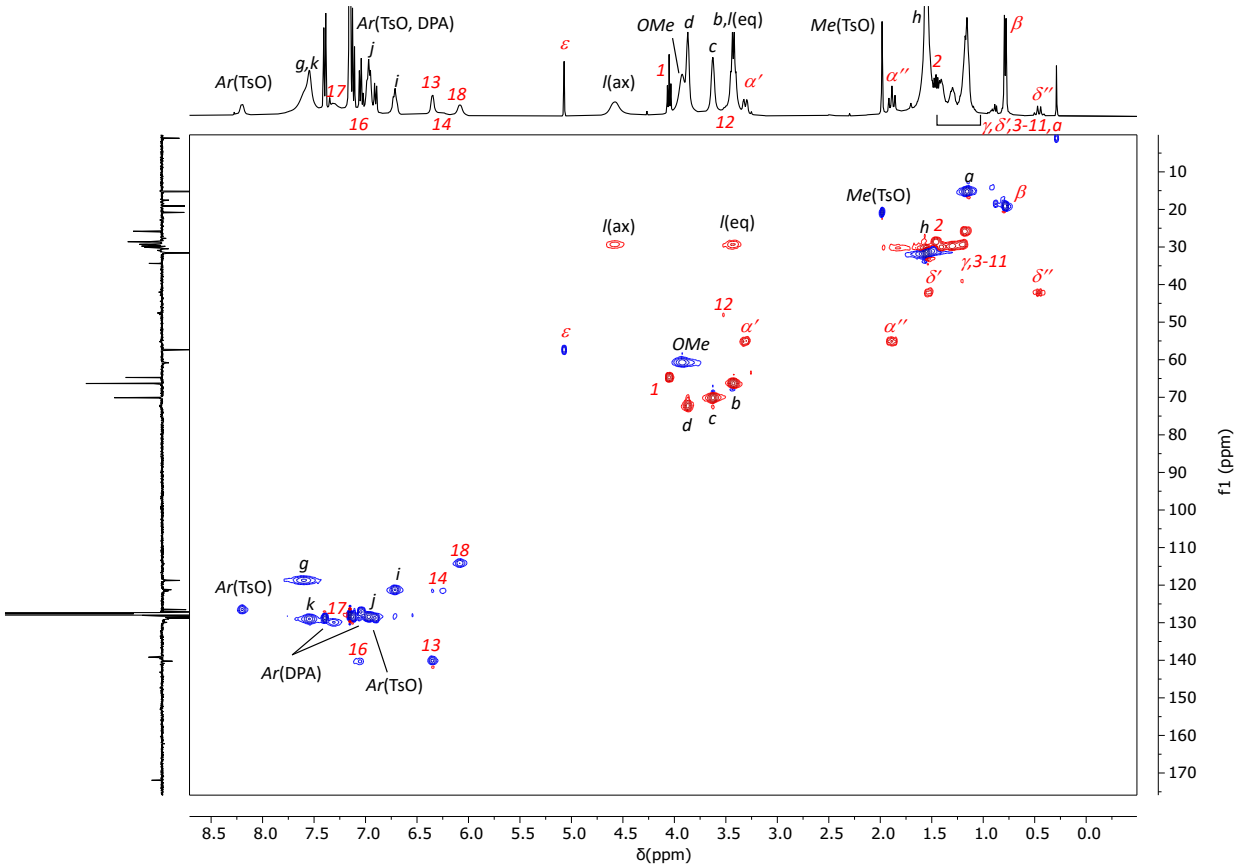

Figure S12: 2D edited-HSQC NMR spectrum of compound **1-Up** (400 MHz, C_6D_6, 25 °C). Blue contours identify CH correlations in CH_3 and CH groups, while red contours show those in CH_2 groups.

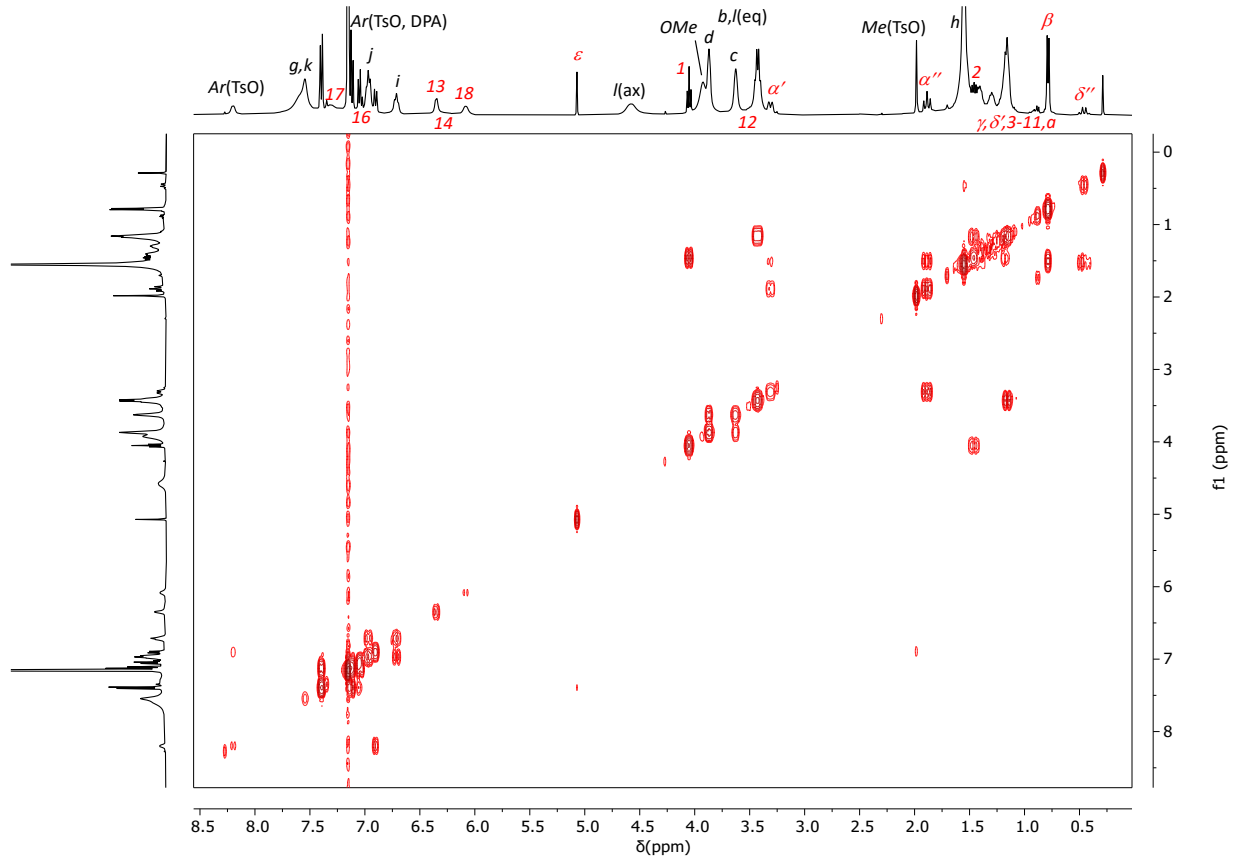

Figure S13: 2D *g*-COSY NMR spectrum of compound **1-Up** (400 MHz, C_6D_6, 25 °C).

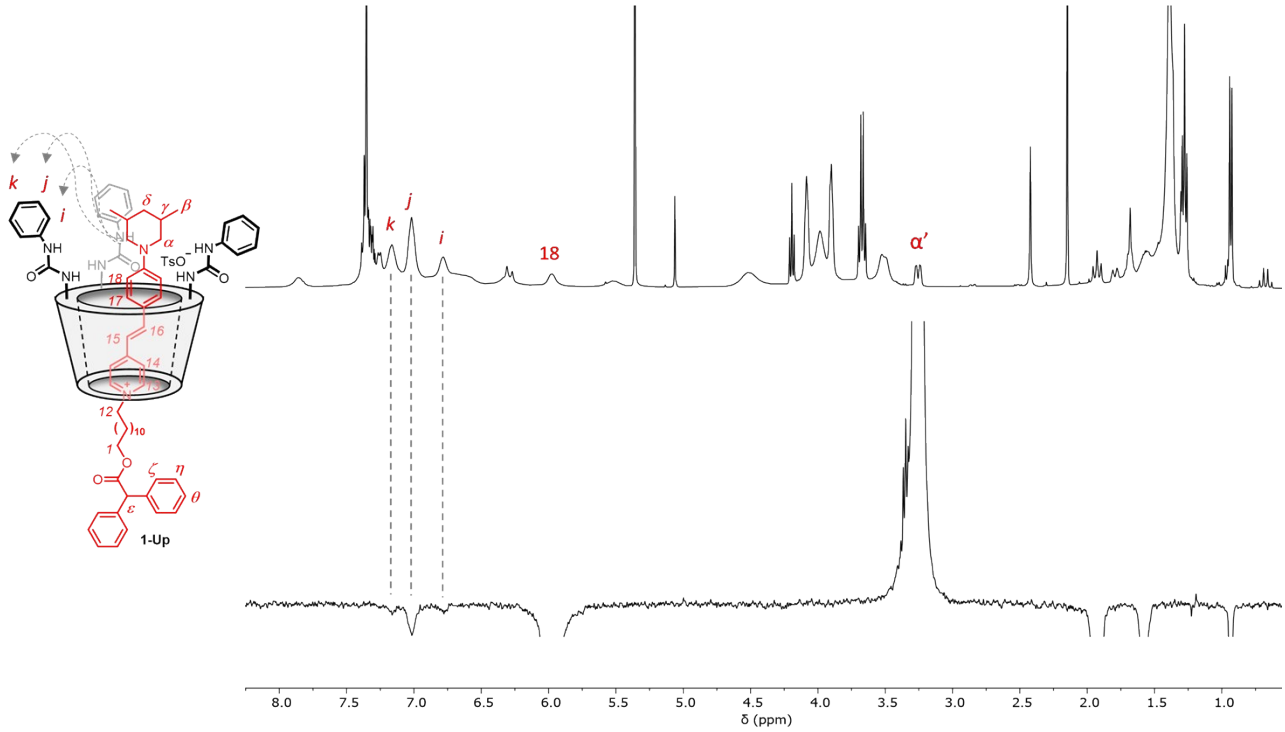

Figure S14: Stack plot of (top) ^{1}H NMR and (down) 1D ROESY of **1-Up** (C_6D_6, 400 MHz, 298 K, Spin-lock = 200 ms). The grey dashed lines show the spatial proximity between protons *α*' of the axle and protons *i*, *j* and *k* of calix[6]arene **3**.

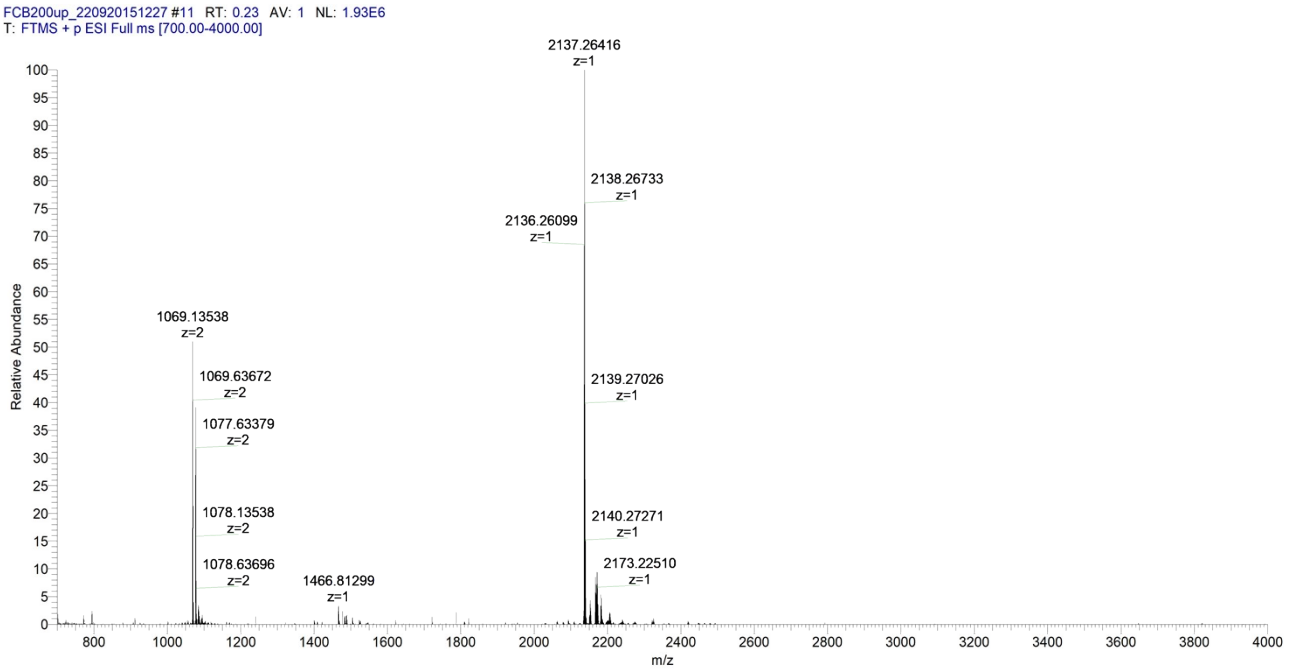

Figure S15: HR-MS (ESI-Orbitrap LQ, positive mode) spectrum of **1-Up**.

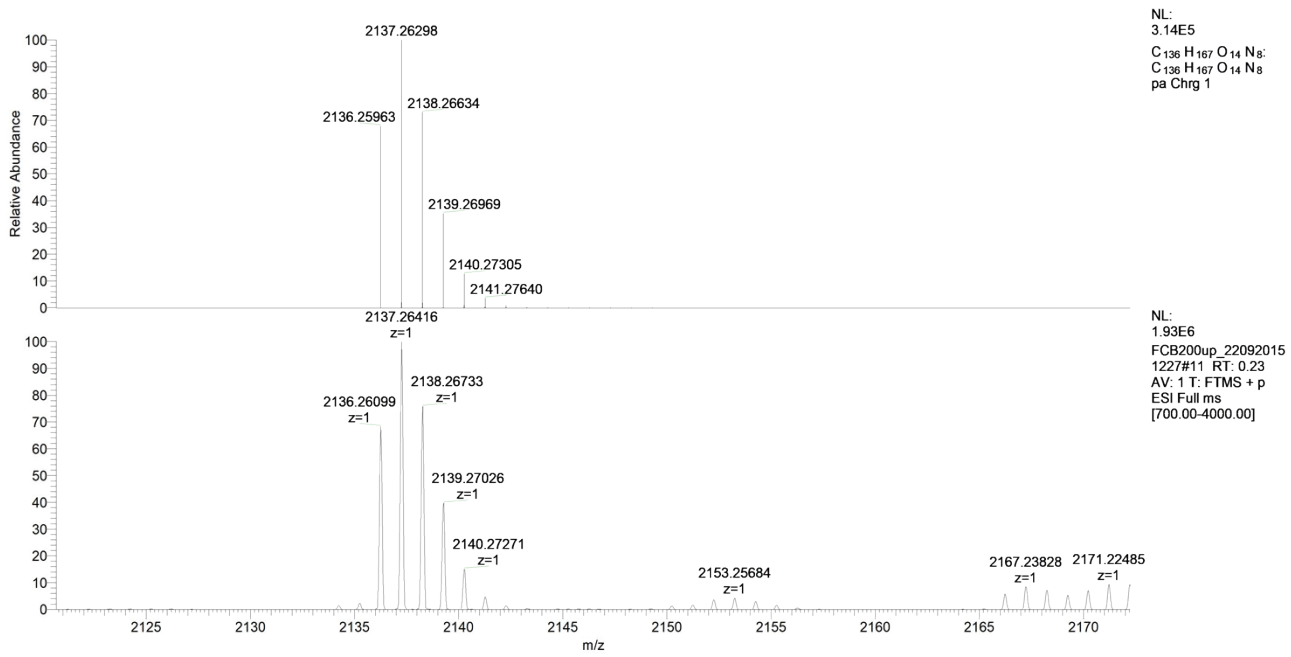

Figure S16: Theoretical (top) and experimental (down) isotopic distribution for the singly charged (z = 1) molecular ion of **1-Up**.

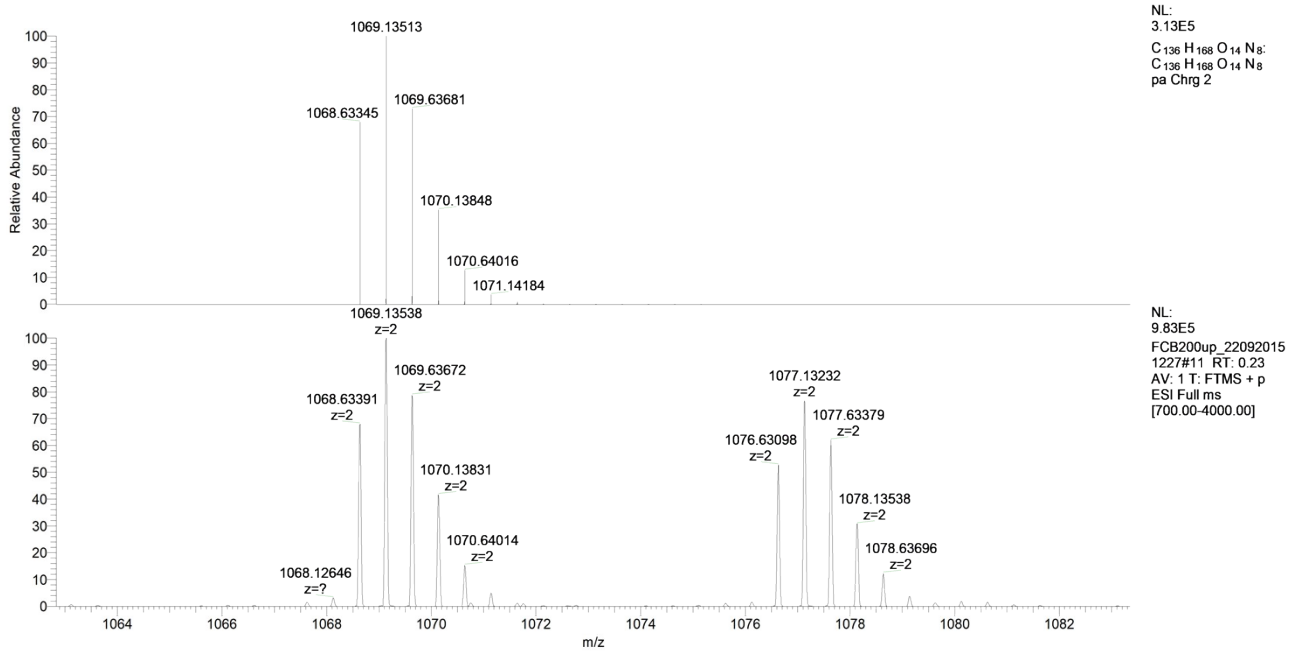

Figure S17: Theoretical (top) and experimental (down) isotopic distribution for the doubly charged (z = 2) molecular ion of **1-Up**.

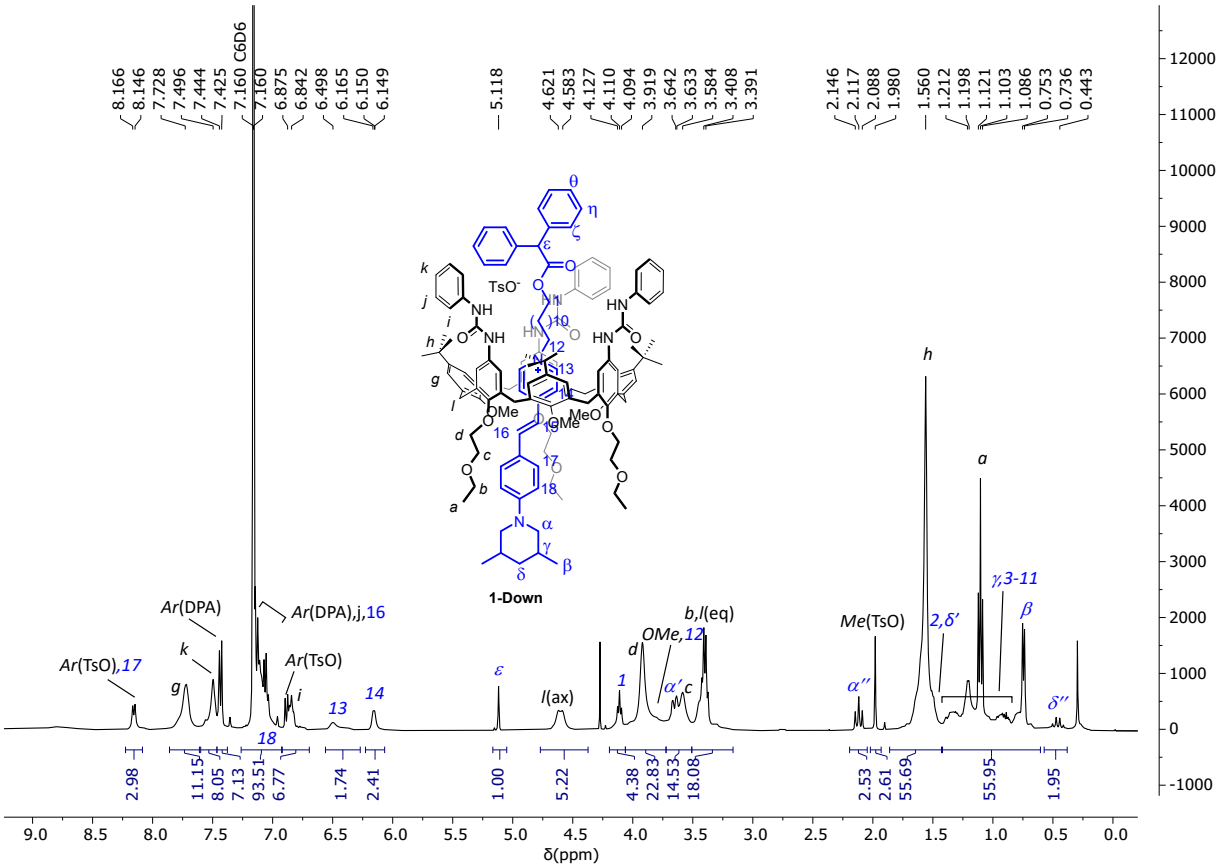

Figure S18: ^{1}H NMR spectrum of compound **1-Down** (400 MHz, C_6D_6, 25 °C).

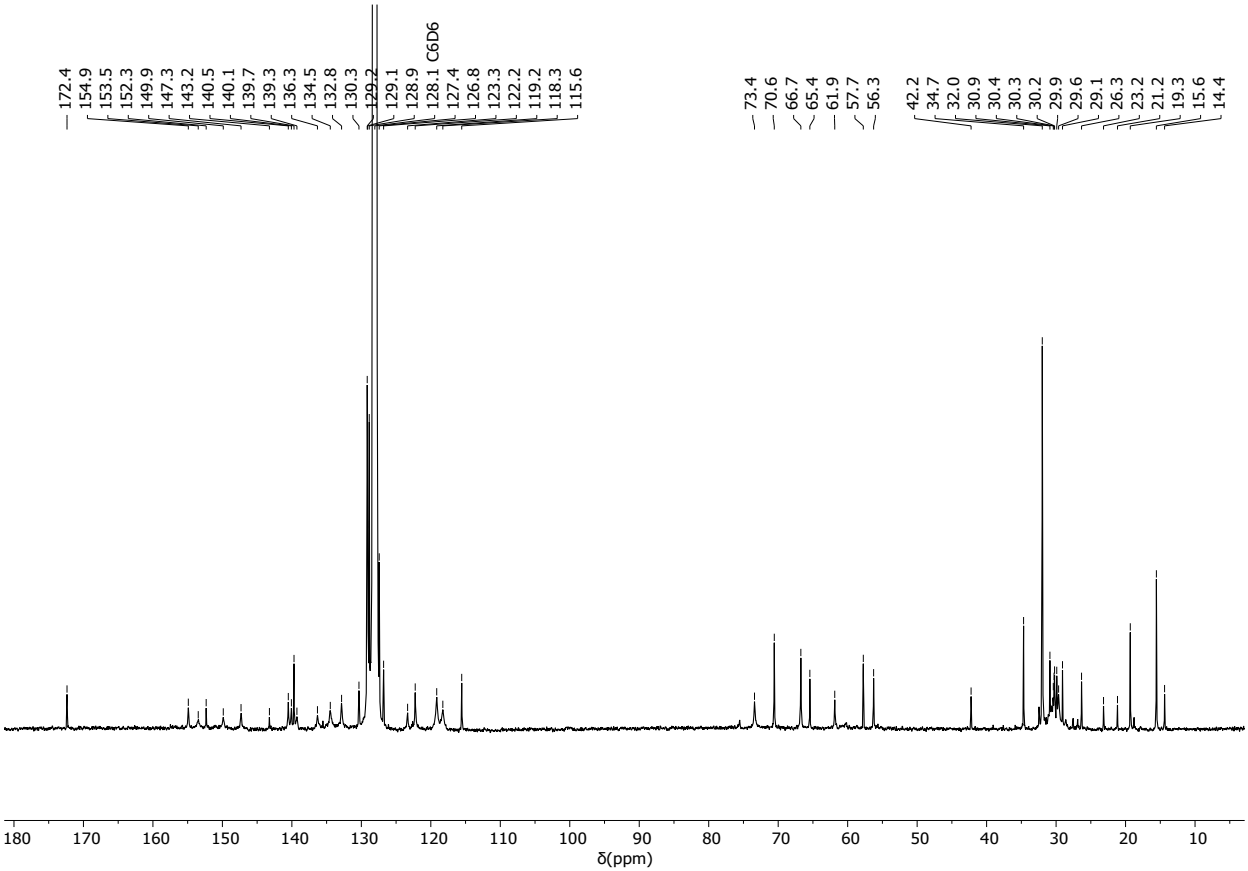

Figure S19: ^{13}C NMR spectrum of compound **1-Down** (100 MHz, C_6D_6, 25 °C).

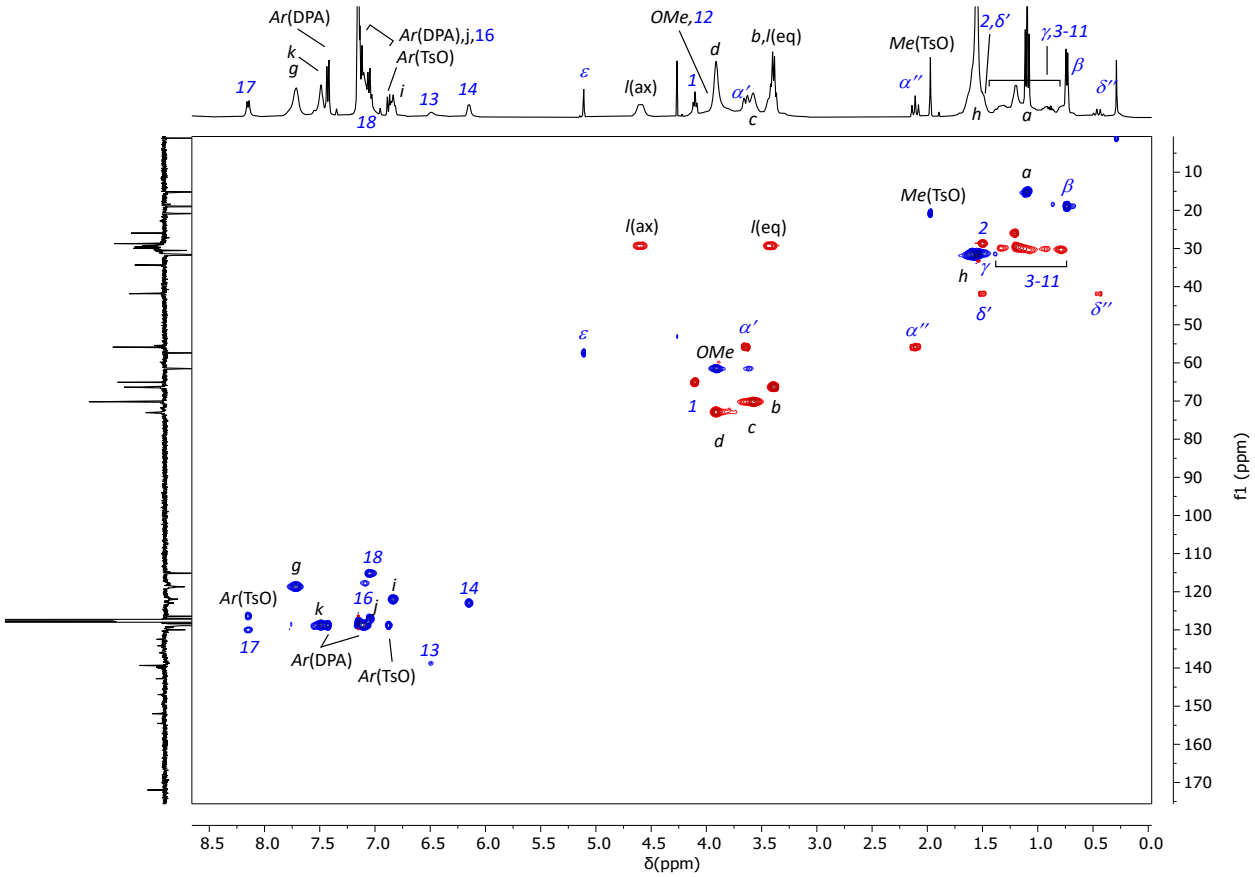

Figure S20: 2D edited-HSQC NMR spectrum of compound **1-Down** (400 MHz, C_6D_6, 25 °C). Blue contours identify CH correlations in CH_3 and CH groups, while the red contours show those in CH_2 groups.

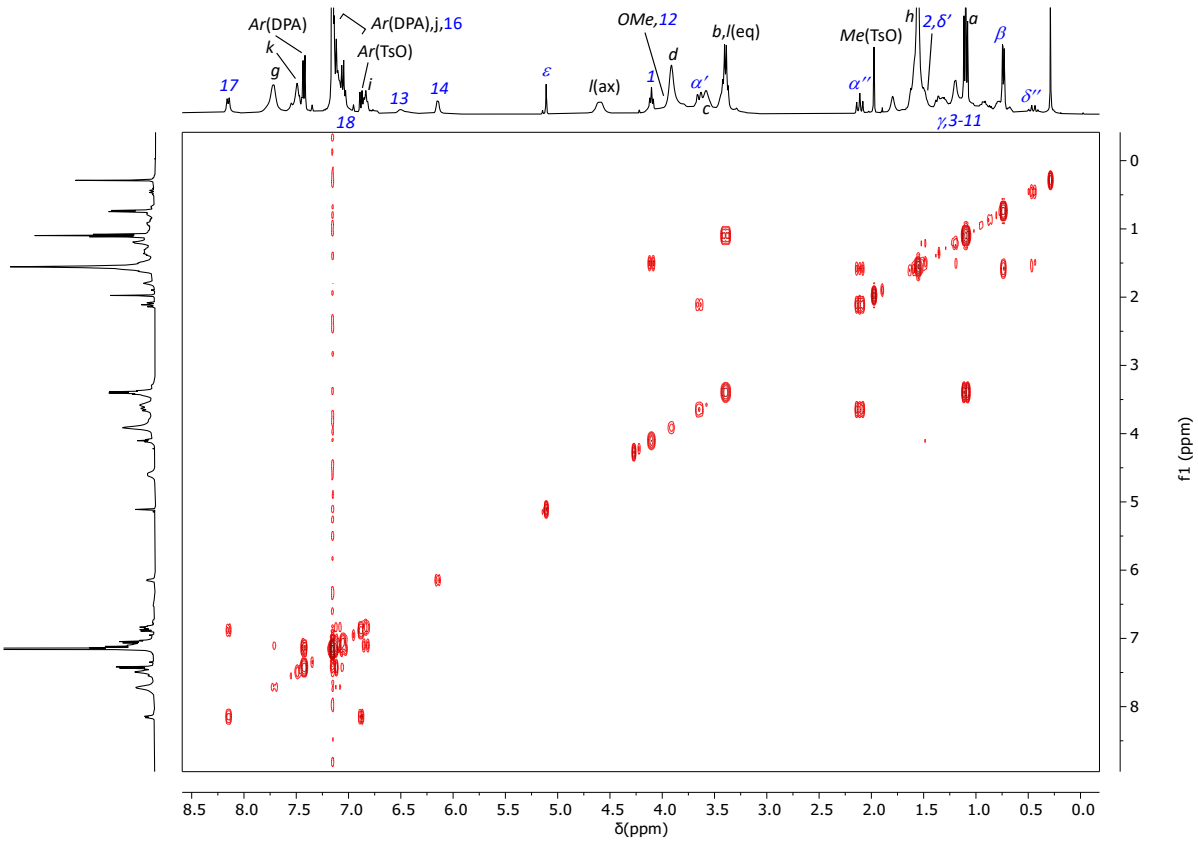

Figure S21: 2D g-COSY NMR spectrum of compound **1-Down** (400 MHz, C_6D_6, 25 °C).

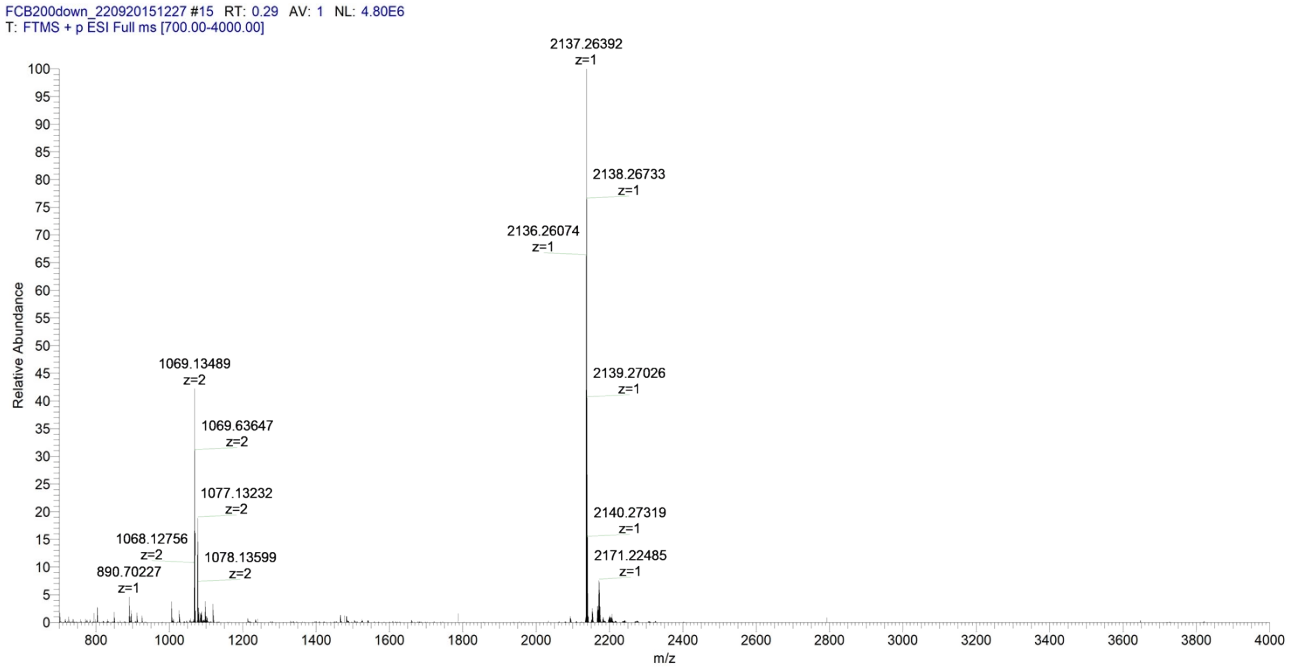

Figure S22: HR-MS (ESI-Orbitrap LQ, positive mode) spectrum of **1-Down**.

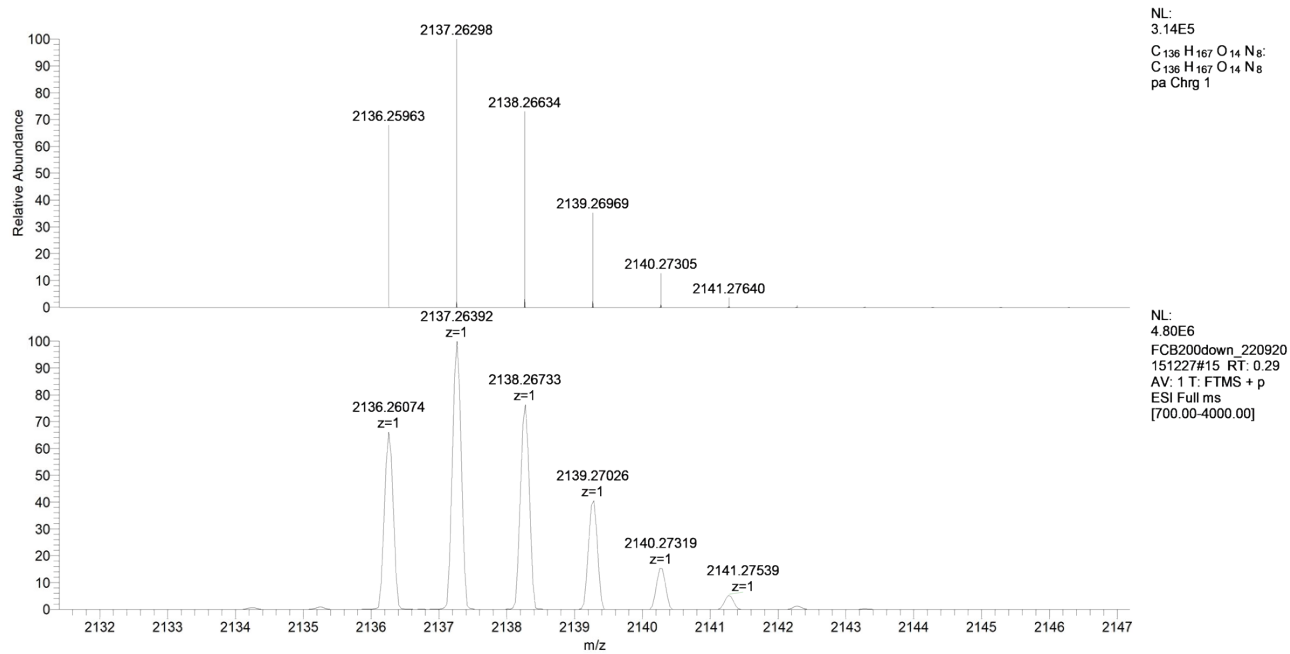

Figure S23: Theoretical (top) and experimental (down) isotopic distribution for the singly charged (z = 1) molecular ion of **1-Dowwn**.

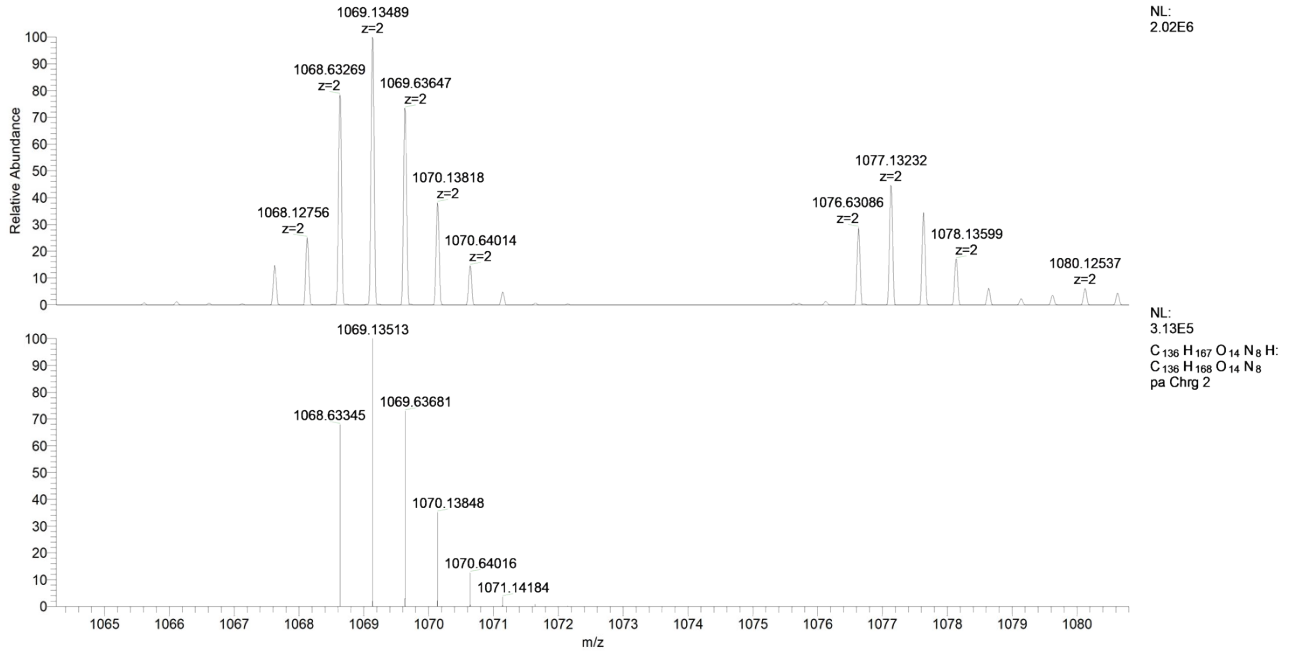

Figure S24: Experimental (top) and theoretical (down) isotopic distribution for the doubly charged (z = 2) molecular ion of **1-Down**.

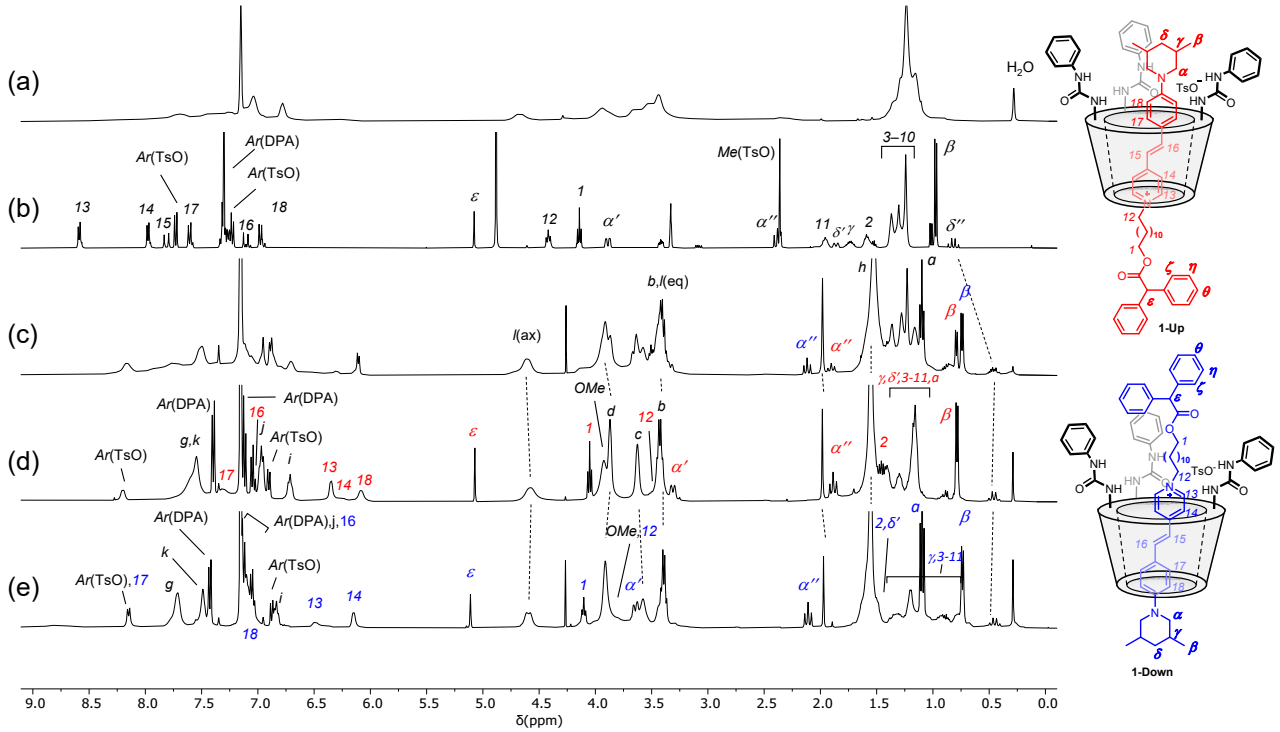

Figure S25: [1] H NMR stack plot (400 MHz) of (a) calix[6]arene **3**, (b) axle **2**, (c) ca. 1:1 mixture of orientational pseudorotaxane isomers **P-Up** and **P-Down**, (d) rotaxane **1-Up**, and (e) rotaxane **1-Down**. All the spectra were taken in C_6D_6 except **2** that was recorded in CD_3OD for solubility reason. For the axle proton signals assignment, see the sketches on the right; for the calix[3]arene **3** proton assignment, see the sketch in Figure 1 of the manuscript.

Photophysical characterisation

Influence of ion pair on the photophysical properties

The absorption spectrum of dumbbell **2** was found to be dependent on the concentration: at micromolar concentrations the band is located around 470 nm, and it shifts progressively to shorter wavelengths at higher concentrations. The influence of the ion pair on the photophysical properties of stilbazolium salts has already been reported,[11,12] therefore it was hypothesised that this effect was related to the ion pairing equilibrium between the stilbazolium ion and its tosylate counterion.

Spectra at increasing concentrations of **2** were recorded, and the data were fitted with a 1:1 model using Hyperquad,[13] obtaining an association constant of 2.0×10^5 M^{-1}.

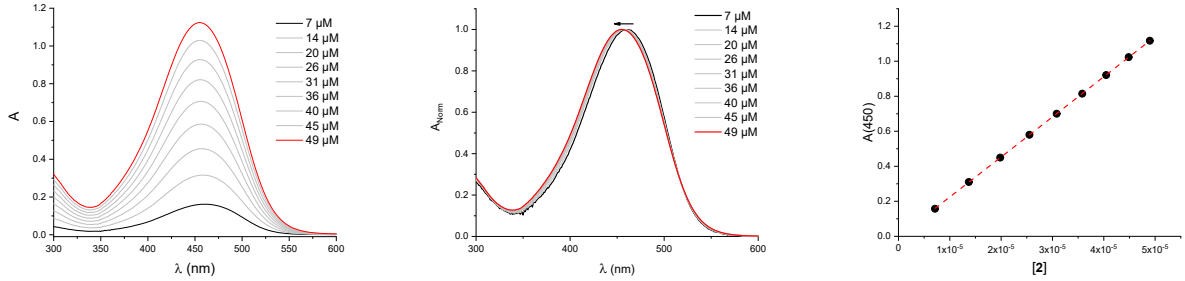

Figure S26. Left: Absorption spectra of a toluene solution of **2** (black to red lines) at increasing concentrations. Centre: Normalised absorption spectra of a toluene solution of **2** (black to red lines) at increasing concentrations. Right: Absorption changes at 450 nm (black dots) together with the fitting of the data (red dashed line).

In order to verify our hypothesis, a large excess of tetrabutylammonium tosylate (TBAOTs) was added to a diluted solution of **2**: a blueshift of the band was observed, and the new spectrum matches well with the one calculated for the ion-paired **2** during the fitting.

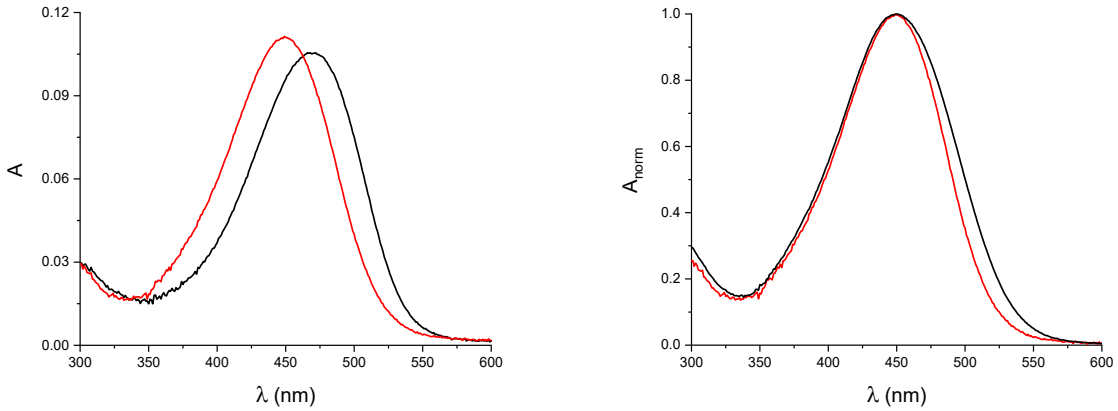

Figure S27. Right: Absorption spectra of a toluene solution of **2** (5×10^{-6} M, black line) and of the same solution upon addition of 1000 equivalents of TBAOTs (red line). Left: Normalised absorption spectra of a toluene solution of **2** + 1000 equivalents of TBAOTs (black line) and of ion-paired **2** calculated by Hyperquad (red line).

The emission spectrum of **2** is also influenced by the ion pair. Upon addition of an excess of TBAOTs to a diluted solution of **2**, the emission is redshifted, and Φ_f increases from 7% to 18%. Due to the association constant of 2.0×10^5 M^{-1}, a non-negligible amount of ion-paired **2** is present even at micromolar

concentrations. As a consequence, the emission spectrum of a diluted solution of **2** is the sum of the two emitting species (**2** and ion-paired **2**).

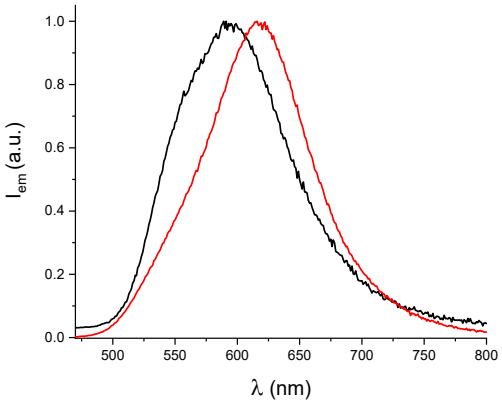

Figure S28. Normalised emission spectra of a toluene solution of **2** (5×10^{-6} M, λ_{ex}= 456 nm black line) and **2** + 1000 equivalents of TBAOTs (5×10^{-6} M, λ_{ex}= 451 nm, red line).

As axle **2** properties are influenced by the ion pairing equilibrium, this compound was studied in the presence of an excess of tosylate counterion to have only one species in solution, i.e. ion-paired **2**.

The absorption spectra of rotaxanes **1-Up** and **1-Down** do not show any dependency on the concentration in the range from 10^{-5} to 10^{-6} M.

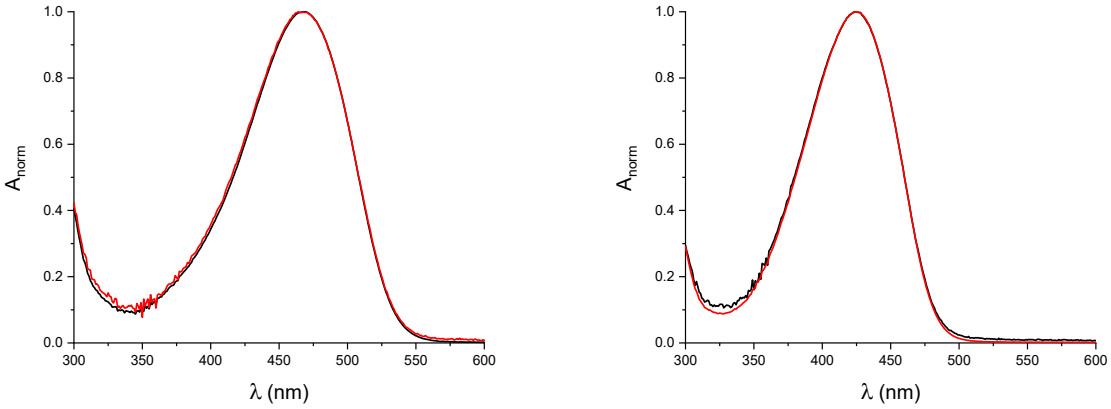

Figure S29. Left: Normalised absorption spectra of a toluene solution of **1-Up** 6.0×10^{-5} M (black line) and 4.8×10^{-6} M (red line). Right: Normalised absorption spectra of a toluene solution of **1-Down** 5.9×10^{-5} M (black line) and 3.1×10^{-6} M (red line).

Photophysical properties

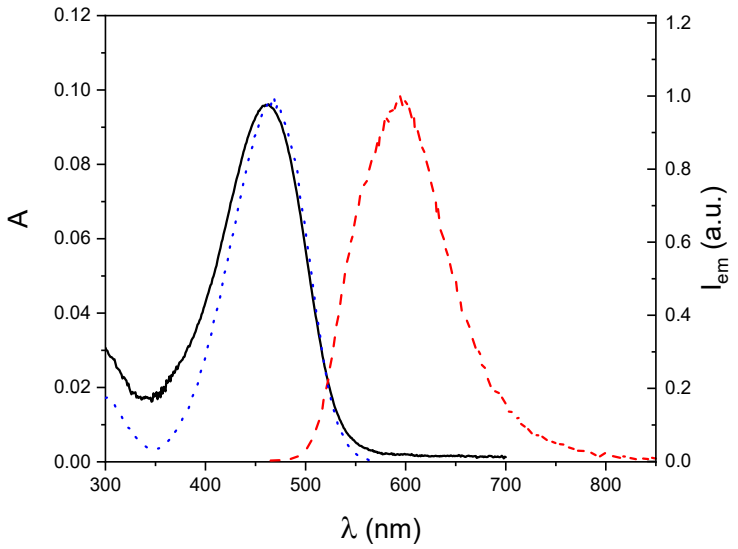

Figure S30. Absorption (black line), emission (λ_{ex}= 456 nm, red dashed line) and excitation (λ_{em}= 595 nm, blue dotted line) spectra of a toluene solution of axle **2** (4.5×10^{-6} M).

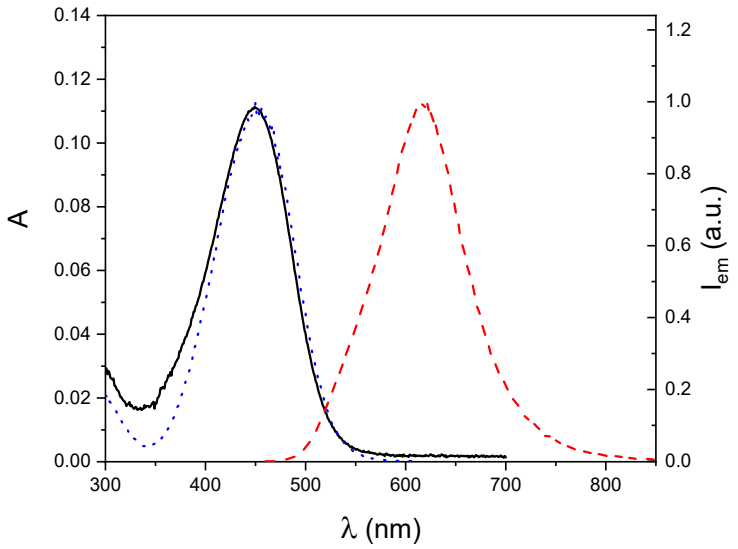

Figure S31. Absorption (black line), emission (λ_{ex}= 451 nm, red dashed line) and excitation (λ_{em}= 618 nm, blue dotted line) spectra of a toluene solution of axle **2** + 1000 equivalents of TBAOTs (5.0×10^{-6} M).

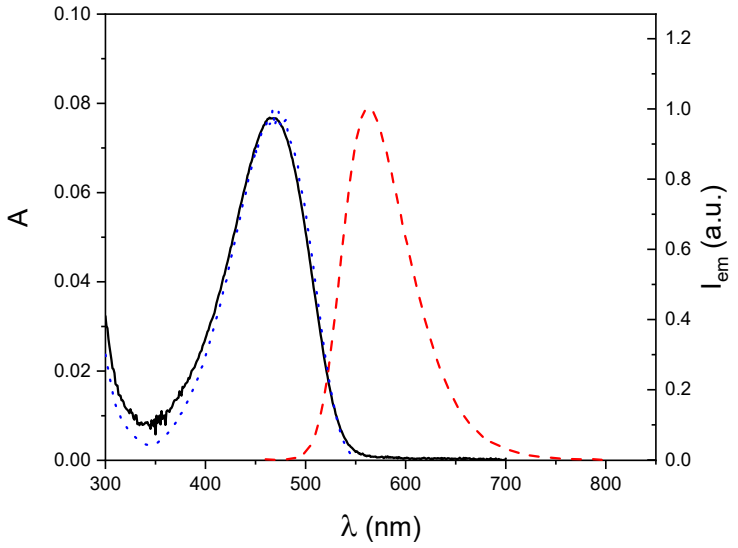

Figure S32. Absorption (black line), emission (λ_{ex}= 454 nm, red dashed line) and excitation (λ_{em}= 561 nm, blue dotted line) spectra of a toluene solution of **1-Up** (3.0×10^{-6} M).

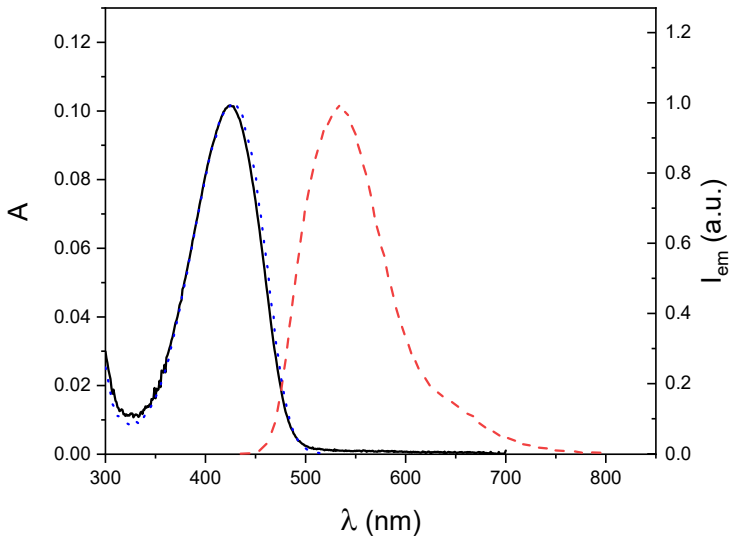

Figure S33. Absorption (black line), emission (λ_{ex}= 425nm, red dashed line) and excitation (λ_{em}= 534nm, blue dotted line) spectra of a toluene solution of **1-Down** (3.1×10^{-6} M).

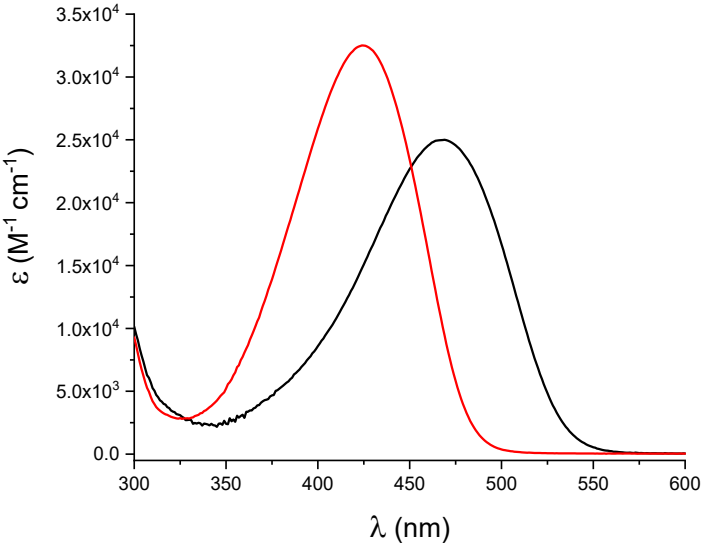

Figure S34. Absorption spectra of **1-Up** (black line) and **1-Down** (red line) in toluene.

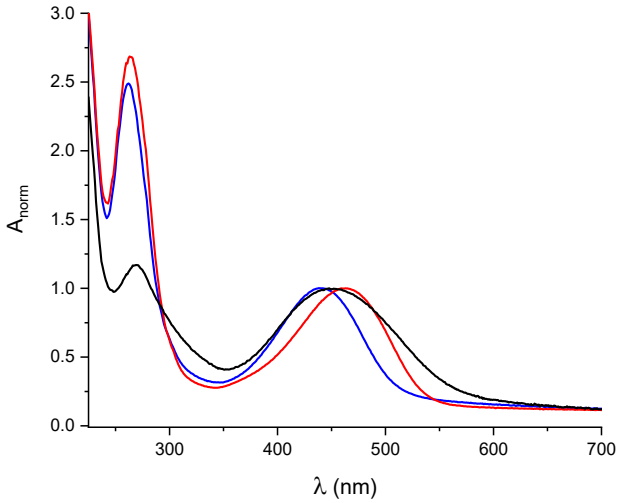

Figure S35. Normalised absorption spectra of solid films of axle **2** (black line), **1-Up** (red line) and **1-Down** (blue line).

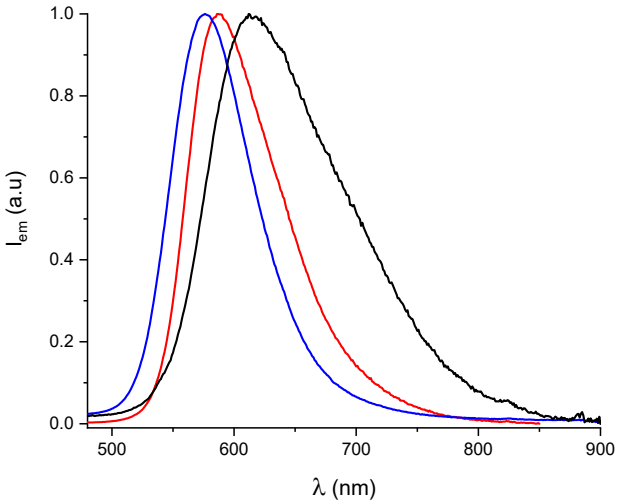

Figure S36. Normalised emission spectra of solid axle **2** (black line), solid **1-Up** (red line) and solid **1-Down** (blue line).

Photochemical characterisation

Determination of the Z isomer spectra

The spectrum of *Z* **1-Down** was calculated using the method reported by Fischer[14] using the two photostationary states (PSS) produced upon irradiation at 365 nm and 436 nm. The method was repeated using another couple of PSS at 365 nm and 405 nm, and the two calculated spectra were averaged.

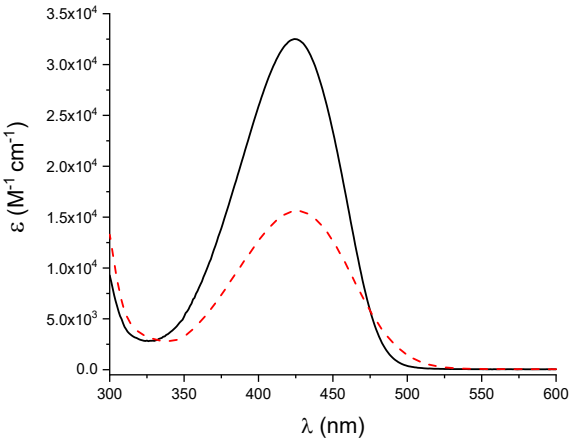

Figure S37. Absorption spectrum in toluene of *E* **1-Down** (full black line) and calculated absorption spectrum of *Z* **1-Down** (red dashed line).

The spectrum of *Z* **1-Up** could not be obtained using the same method. Nevertheless, the shape of the absorption spectrum of **1-Up** changes during the irradiation, and two isosbestic points are present at 333 nm and 531 nm. At the same time, the shape of the excitation and emission spectra and the fluorescence lifetime do not change upon irradiation. Therefore, we hypothesised that the emission of the *Z* isomer is negligible with respect to that of the *E* isomer. This assumption allowed us to estimate the percentage of the *Z* isomer in an irradiated solution of **1-Up**, from the decrease in emission intensity obtained after irradiation at 436 nm and to calculate the *Z* isomer spectrum.

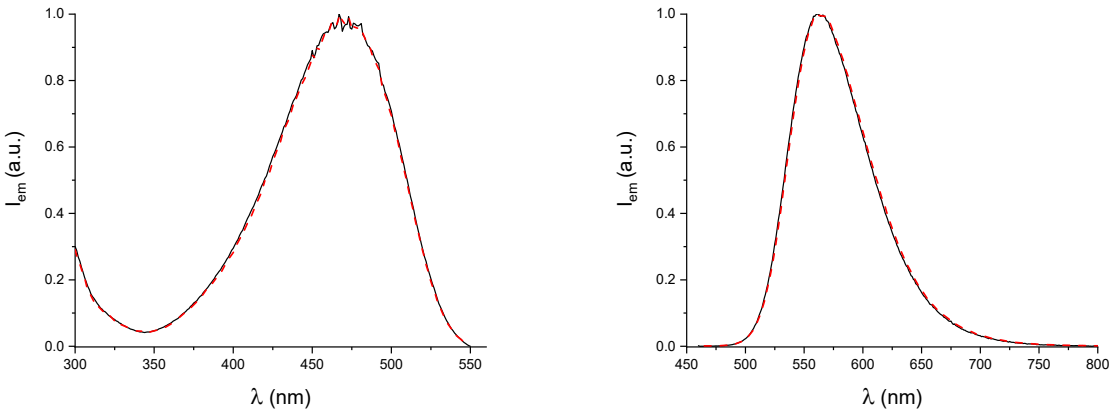

Figure S38. Left: Normalised excitation spectra of toluene solutions of **1-Up** (3.0×10^{-6} M, λ_{em}= 561 nm, full black line) and of **1-Up** irradiated at 436 nm to the photostationary state (4.0×10^{-6} M, λ_{em}= 565 nm, red dashed line). Right: Normalised emission spectra of toluene solutions of **1-Up** (3.0×10^{-6} M, λ_{ex}= 454 nm, full black line) and **1-Up** irradiated at 436 nm to the photostationary state (4.0×10^{-6} M, λ_{ex}= 457 nm, red dashed line).

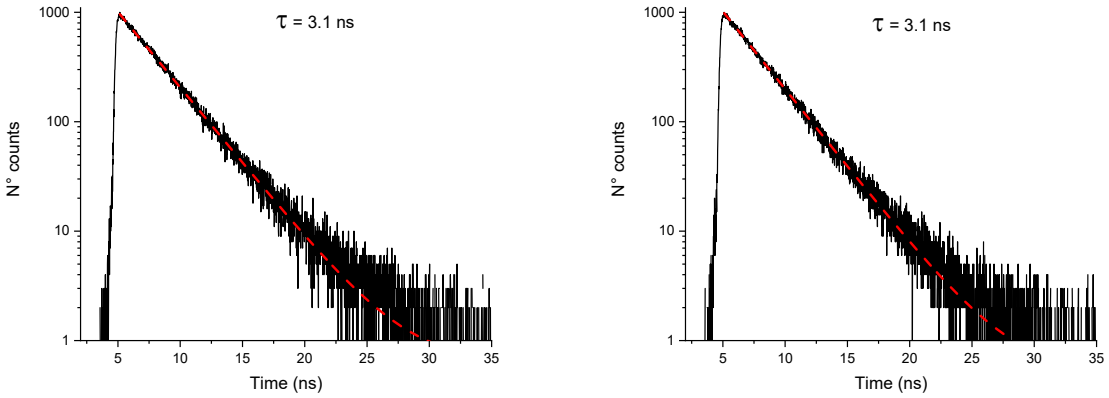

Figure S39. Fluorescence decay curves (black lines) of toluene solutions of **1-Up** (left, 3.0×10^{-6} M, λ_{em}= 561 nm) and of **1-Up** irradiated at 436 nm to the photostationary state (right, 4.0×10^{-6} M, λ_{em}= 565 nm). The red dashed line represents the data fitting.

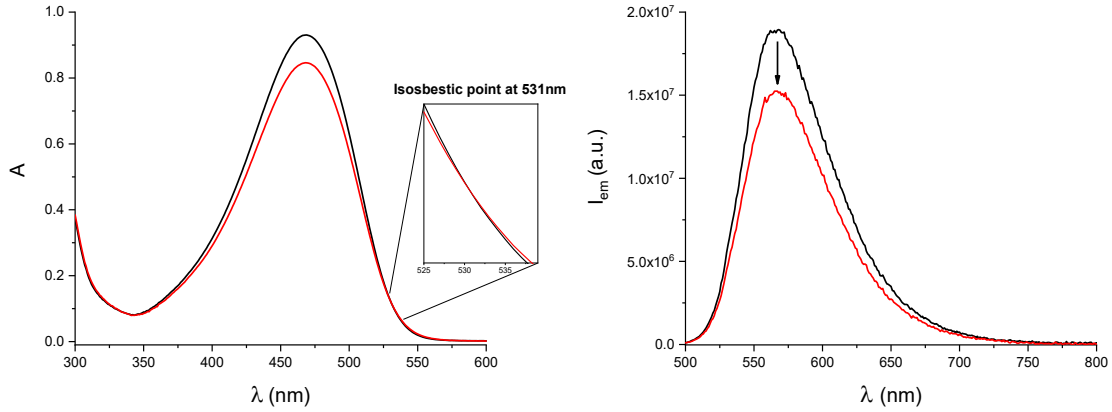

Figure S40. Absorption (left) and emission (right) spectra of a toluene solution of **1-Up** (3.7×10^{-5} M, λ_{ex}= 531 nm, black line) and of the same solution upon irradiation at 436 nm (λ_{ex}= 531 nm, red line).

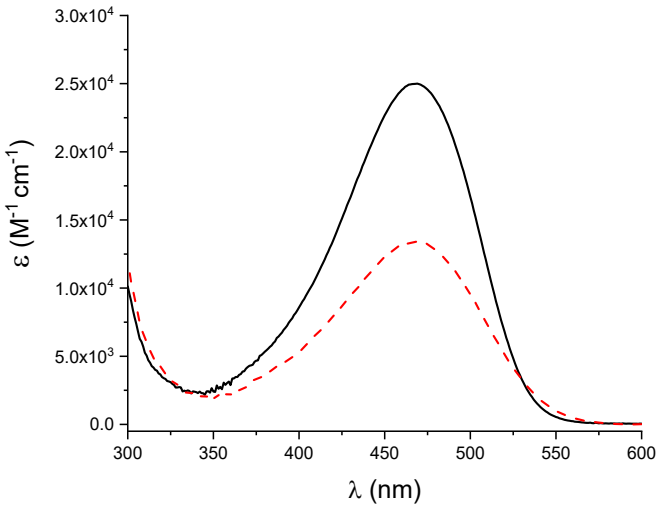

Figure S41. Absorption spectrum in toluene of *E* **1-Up** (full black line) and calculated absorption spectrum of *Z* **1-Up** (red dashed line).

It is assumed that *Z* **2** displays an ion pairing equilibrium similar to *E* **2** and that, in the presence of an excess of tosylate, such equilibrium is shifted toward the formation of the ion pair. The spectrum of ion-paired *Z* **2** could not be obtained using the Fischer method. Methods based on the analysis of the thermal back isomerisation spectra by Multivariate Curve Resolution (MCR)[15] failed as well in calculating the *Z* isomer spectrum, probably due to the high similarity between the spectra of the *E* and *Z* isomers. It was observed that, for **1-Up** and **1-Down**, the *Z* isomer spectrum is characterised by an absorption coefficient at the maximum of the band which is around half of that of the *E* isomer. A similar behaviour was assumed to be true for ion-paired *Z* **2**, i.e. $\varepsilon_Z \approx \frac{1}{2}\,\varepsilon_E$ was used as a guess for the spectrum of the Z isomer; this value was then optimised during the fitting of the photokinetics, allowing to determine the spectrum of the Z isomer. In order to verify that the assumption made was plausible, the fitting was repeated leaving ε_Z completely free to vary (and thus not using the guess based on the abovementioned assumption): a very similar value was obtained for ε_Z, and the fitting gave results comparable to the previous case.

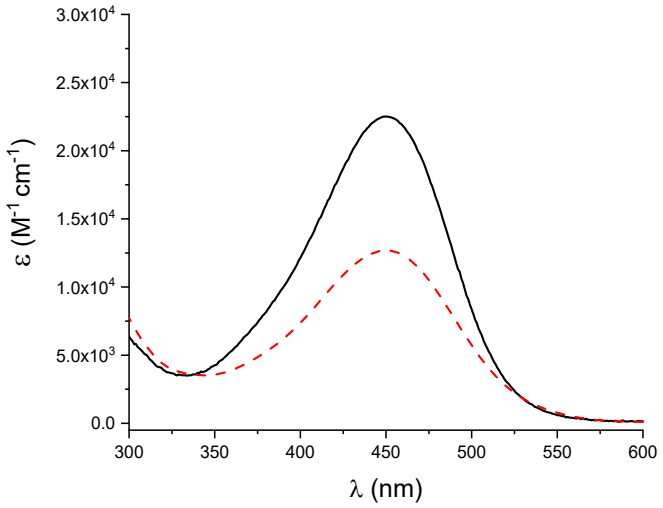

Figure S42. Absorption spectrum in toluene of ion-paired *E* **2** (full black line) and calculated absorption spectrum of ion-paired *Z* **2** (red dashed line).

Photoisomerisation quantum yield measurements

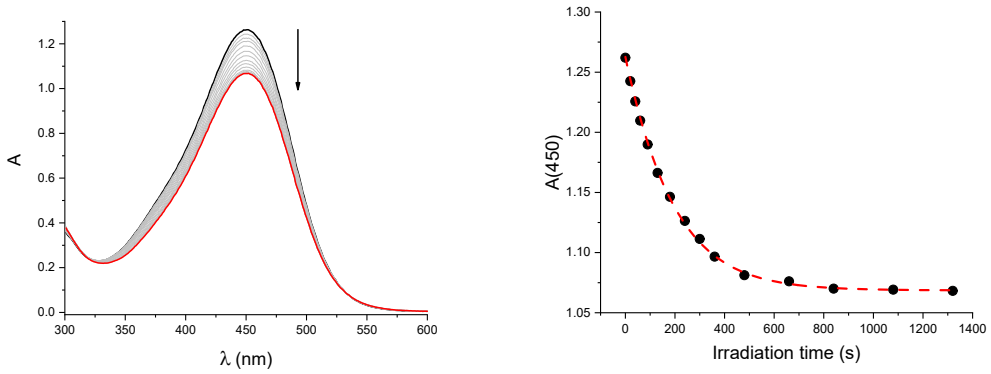

Figure S43. Left: Time-dependent absorption spectra of a toluene solution of *E* **2** + 500 equivalents of TBAOTs (5.5×10^{-5} M, black to red lines) upon irradiation at 436 nm. Right: Absorption changes at 450 nm (black dots) together with the fitting of the data (red dashed line).

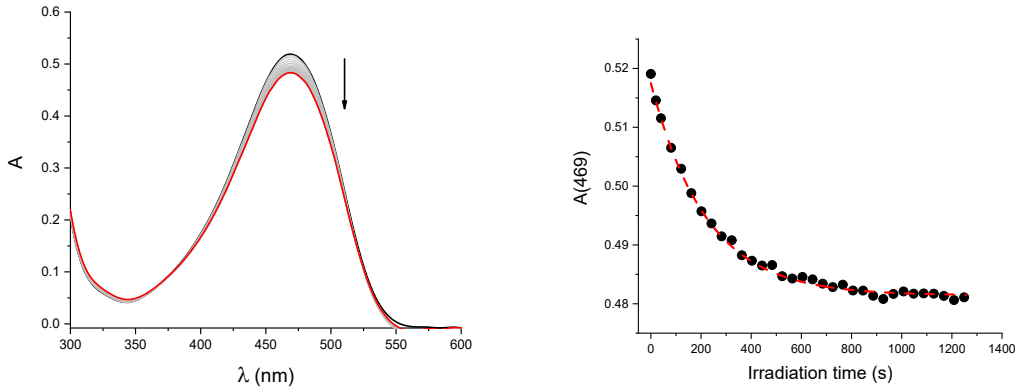

Figure S44. Left: Time-dependent absorption spectra of a toluene solution of *E* **1-Up** (2.1×10^{-5} M, black to red lines) upon irradiation at 436 nm. Right: Absorption changes at 469 nm (black dots) together with the fitting of the data (red dashed line).

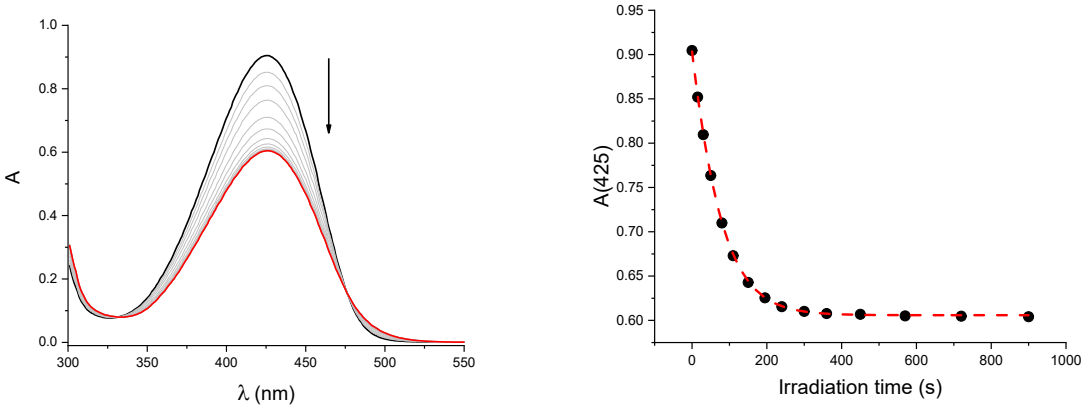

Figure S45. Left: Time-dependent absorption spectra of a toluene solution of *E* **1-Down** (2.8×10^{-5} M, black to red lines) upon irradiation at 436 nm. Right: Absorption changes at 425 nm (black dots) together with the fitting of the data (red dashed line).

Thermal back isomerisation kinetics

The thermal back isomerisation of ion-paired **2** follows a first-order kinetics with a kinetic constant k= 2.7 × 10^{-4} s^{-1}.

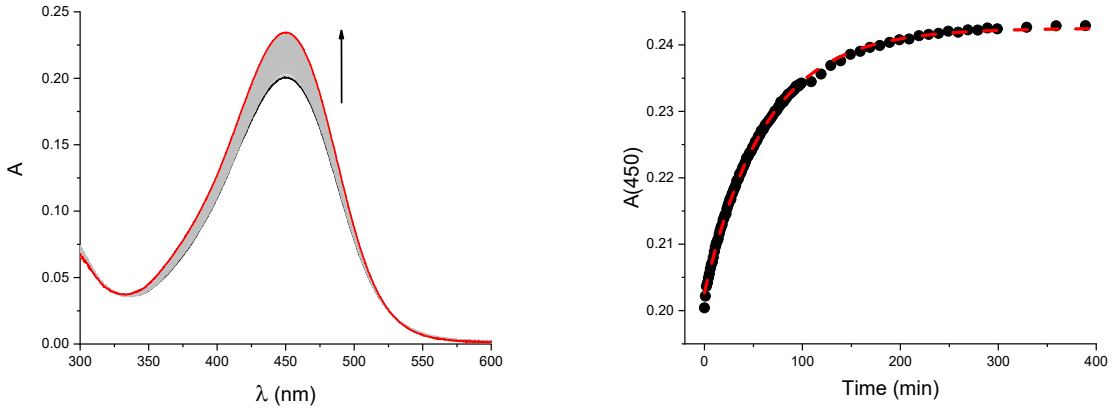

Figure S46. Left: Time-dependent absorption spectra of a toluene solution of **2** + 1000 equivalents of TBAOTs (1.0 × 10^{-5} M, black to red lines) previously irradiated at 436 nm. Right: Absorption changes at 450 nm (black dots) together with the fitting of the data (red dashed line).

The thermal back isomerisation of **1-Down** is extremely slow and, assuming a first-order kinetics, its rate constant was estimated to be k ≃ 5 × 10^{-8} s^{-1}. To do so, the logarithm of the concentration of *Z*-**1-Down** over time was linearly fitted according to the equation:

$$\ln[Z-\mathbf{1\text{-}Down}] = [Z-\mathbf{1\text{-}Down}]_0 - kt$$

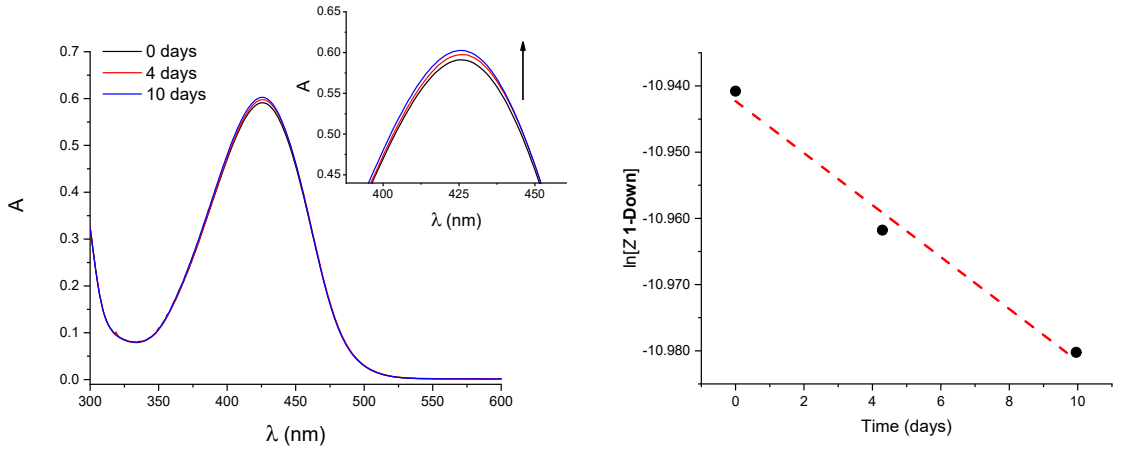

Figure S47. Left: Time-dependent absorption spectra of a toluene solution of **1-Down** (2.7 × 10^{-5} M, black to blue lines) previously irradiated at 436 nm. Right: Concentration changes over time of *Z* **1-Down** (black dots) together with the fitting of the data (red dashed line).

After irradiating a toluene solution of **1-Up**, the initial spectrum is restored within one day, and the related kinetic trace shows the presence of two processes. The kinetic trace was fitted as two first-order parallel reactions, obtaining k_1= 1 × 10^{-4} s^{-1} and k_2= 5 × 10^{-3} s^{-1}. The first process accounts for the large part of absorbance variation (more than 90%), and is ascribed to the thermal *Z* to *E* isomerisation, in analogy with the process observed for axle **2**. The nature of the second process, related to very small absorption changes, is unclear. Due to the minor absorption variation and the fast kinetics (the process is ended in few minutes), the process could not be further investigated.

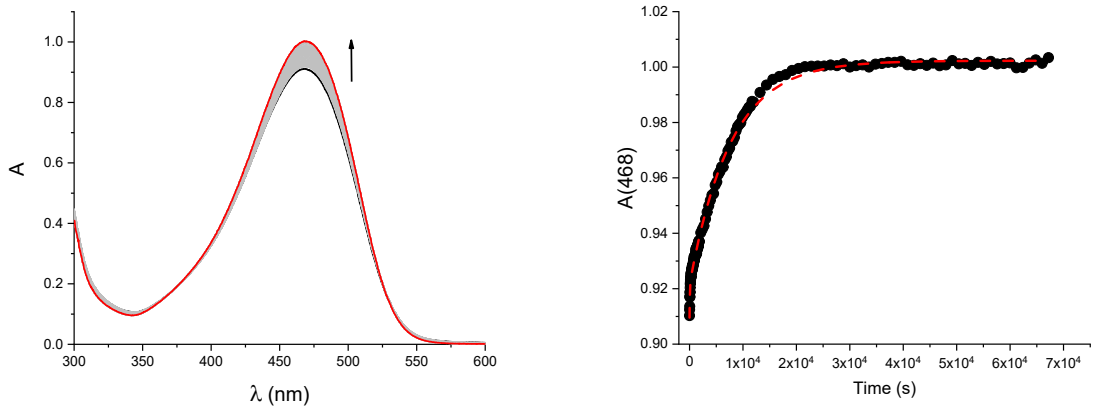

Figure S48. Left: Time-dependent absorption spectra of a toluene solution of **1-Up** (4.0×10^{-5} M, black to blue lines) previously irradiated at 436 nm. Right: Absorption changes at 468 nm (black dots) together with the fitting of the data (red dashed line).

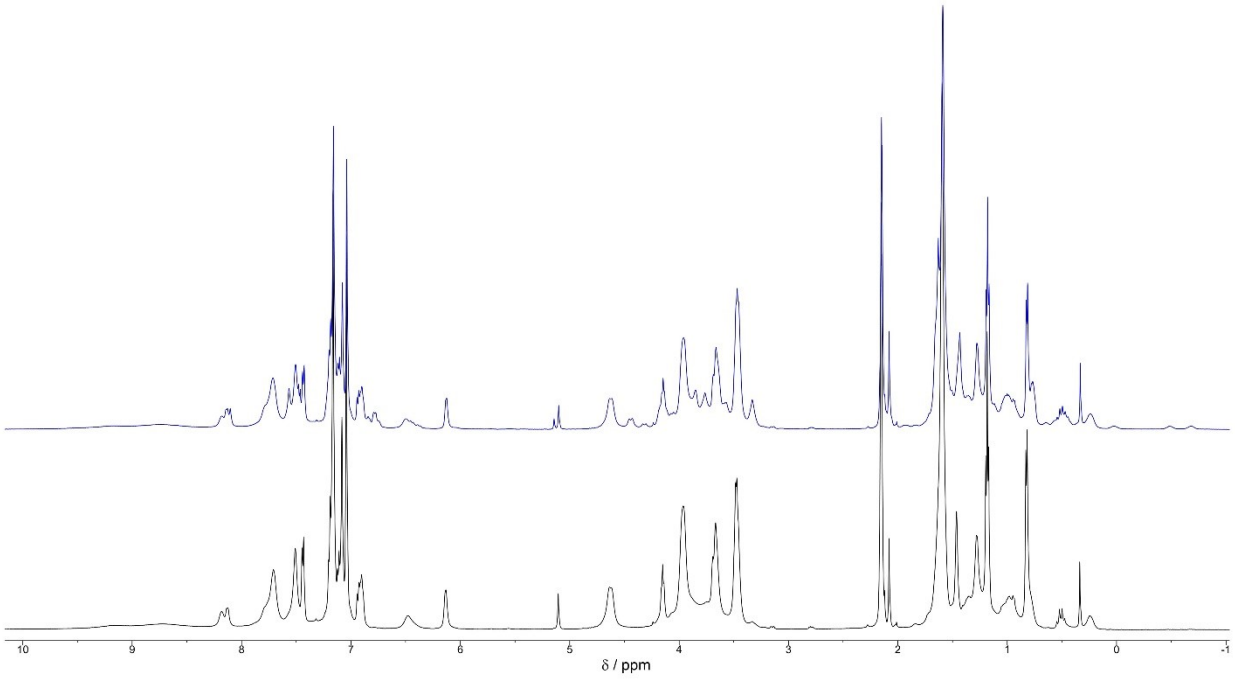

Figure S49. ^{1}H NMR spectra of **1-Down** (500 MHz, toluene-d_8, 25 °C) (black line) and of the same solution after exhaustive irradiation at λ_{irr} ~ 365 nm (blue line). PPS composition 25% *Z* isomer, 75% *E* isomer.

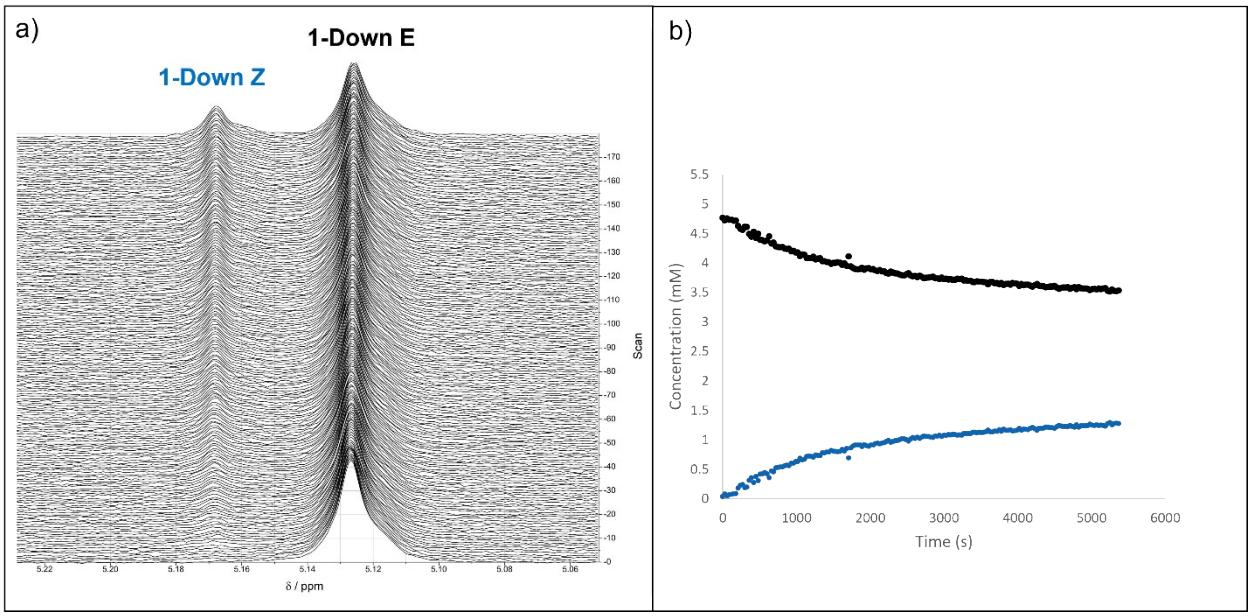

Figure S50. a) Extract of the arrayed ^{1}H NMR spectra of **1-Down** (5 mM, 500 MHz, toluene-d_8, 25 °C) recoded at 30 s intervals under continuous irradiation at λ_{irr} ~ 365 nm. b) Experimental traces showing the variation of concentration of the *E* (black line) and *Z* (blue line) isomer under continuous irradiation. PPS composition 25% *Z* isomer, 75% *E* isomer.

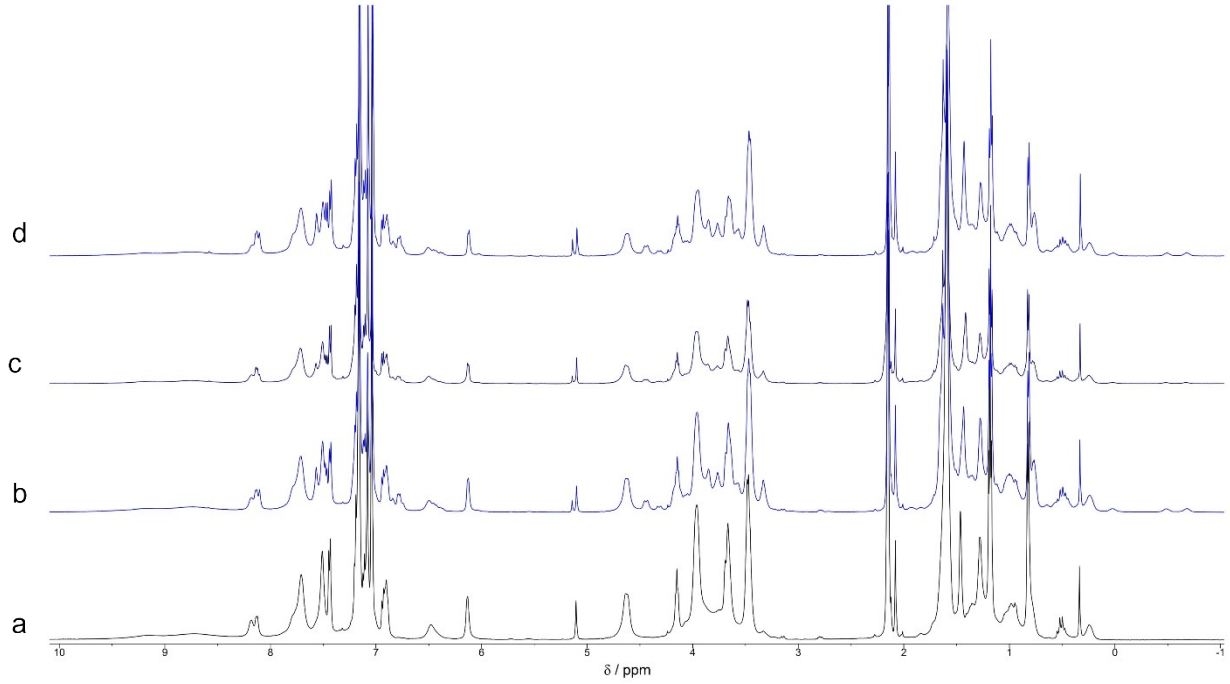

Figure S51. ^{1}H NMR spectra (500 MHz, toluene-d_8, 25 °C) of: a) **1-Down** (5 mM); b) Sample (a) after exhaustive irradiation at λ_{irr} ~ 365 nm; c) Sample (b) after 20 days in the dark; d) Sample (c) after exhaustive irradiation at λ_{irr} ~ 365 nm.

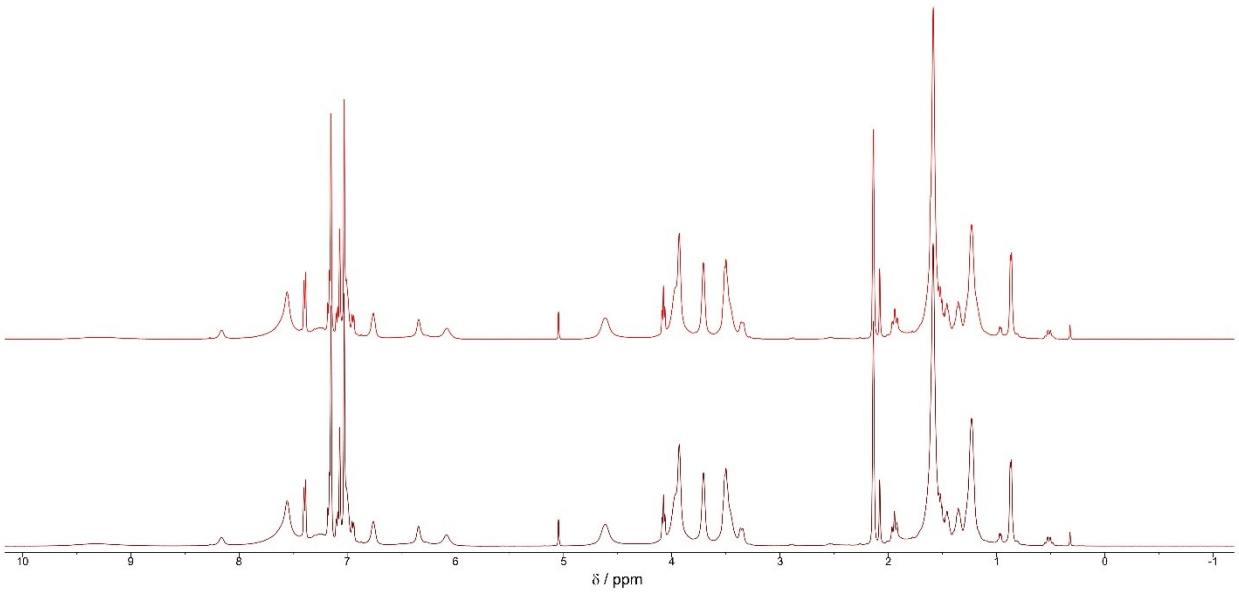

Figure S52. ^{1}H NMR spectra of **1-Up** (500 MHz, toluene-d_8, 25 °C) (brown line) and of the same solution after 110 minutes irradiation at λ_{irr} ~ 460 nm (red line). No *Z* isomer was detected.

X-ray characterization

Refinement Additional Details

Several moieties decorating the calixarene wheel presented significant thermal parameters: the phenyl groups attached to ureido moieties, *tert*-butyl groups and ethyl moieties belonging to OEtOEt arms. Each one was split over two distinct sites (s.o.f. 0.5 : 0.5, except for one ethyl fragment, s.o.f. 0.75 : 0.25) and modelled with a series of restraints (SIMU, ISOR, DFIX, DANG) and EADP constraint. Disordered oxygen atoms were pinpointed in the residual electron density map near the S atom, belonging to the tosylate anion. Since the remaining disordered part (C_7H_7) of the tosylate anion could not be detected in the residual electron density map, the tolyl fragment was refined isotropically on two distinct sites (each one half occupied) with a series of DANG, FLAT, DFIX restraints and AFIX, EADP constraints. The first six CH_2 groups belonging to the C12 chain of the stilbazolium axle were found in the residual electron density map and refined with a full occupancy. Several modelling attempts were performed on the terminal part of the chain, but all of them led to unsatisfactory results. For this reason, only the C7 atom was modelled over two half-occupied sites: C26S and C26g. The terminal piperidine stopper presented quite large thermal parameters, but the splitting over two distinct sites was not satisfactory in this case. Therefore, final refinement was performed with a solvent mask: 1388 electrons were found in a volume of 6051 A^3 per unit cell. This large residual void fraction (36%) hampered the detailed modelling of the terminal part of the guest axle. Hence, the masked residual electron density was taken into account as the terminal part of the axle, and as four additional toluene molecules as crystallization solvent per asymmetric unit.

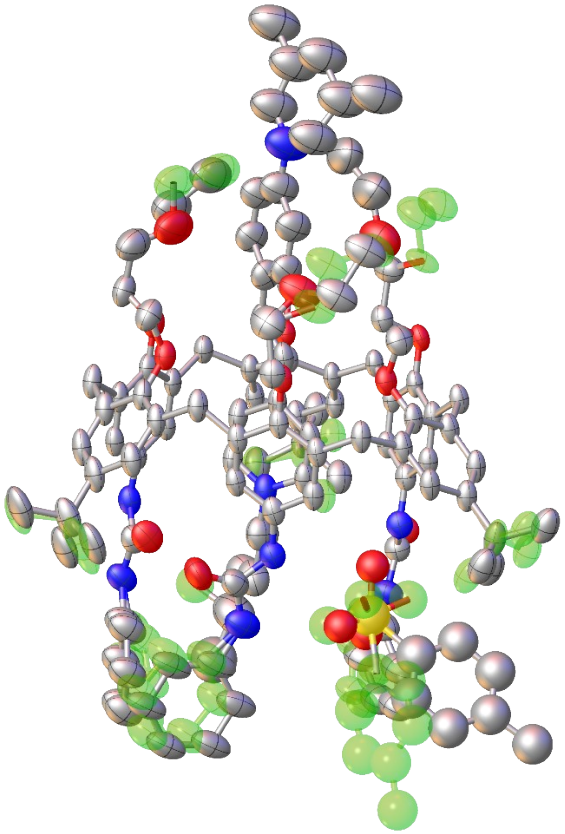

Figure S53. a) Asymmetric unit view of **1-Down**, thermal ellipsoids are plotted at 30% probability level (colour code: C, grey; O, red; N, blue; S, yellow; hydrogen atoms are omitted for clarity). Molecular disorder is represented in shaded green colour.

Table S1. Crystal data and structure refinement for **1-Down**.

Empirical formula	$C_{143}H_{174}N_8O_{17}S$, $4(C_7H_8)$
Formula weight	2677.49
Temperature/K	200.00
Crystal system	monoclinic
Space group	$P2_1/c$
a/Å	23.5888(8)
b/Å	40.7313(7)
c/Å	18.7673(5)
α/°	90
β/°	111.702(3)
γ/°	90
Volume/Å^3	16753.6(9)
Z	4
ρ_{calc}g/cm^3	1.062
μ/mm^{-1}	0.645
F(000)	5760.0
Crystal size/mm^3	0.15 × 0.07 × 0.05
Radiation	CuKα (λ = 1.54184)
2Θ range for data collection/°	4.338 to 140.15
Reflections collected	155184
Independent reflections	31572 [R_{int} = 0.0843, R_{sigma} = 0.0455]
Data/restraints/parameters	31572/876/1352
Goodness-of-fit on F^2	1.074
Final R indexes [I>=2σ (I)]	R_1 = 0.1462, wR_2 = 0.3771
Final R indexes [all data]	R_1 = 0.1945, wR_2 = 0.4262
Largest diff. peak/hole / e Å^{-3}	0.77/-0.43

$R1 = \Sigma||Fo|-|Fc||/\Sigma|Fo|$, $wR_2 = [\Sigma[w(Fo^2-Fc^2)^2]/\Sigma[w(Fo^2)^2]]^{½}$, $w = 1/[\sigma^2(Fo^2) + (aP)^2 + bP]$, where$P = [max(Fo^2,0) + 2Fc^2]/3$

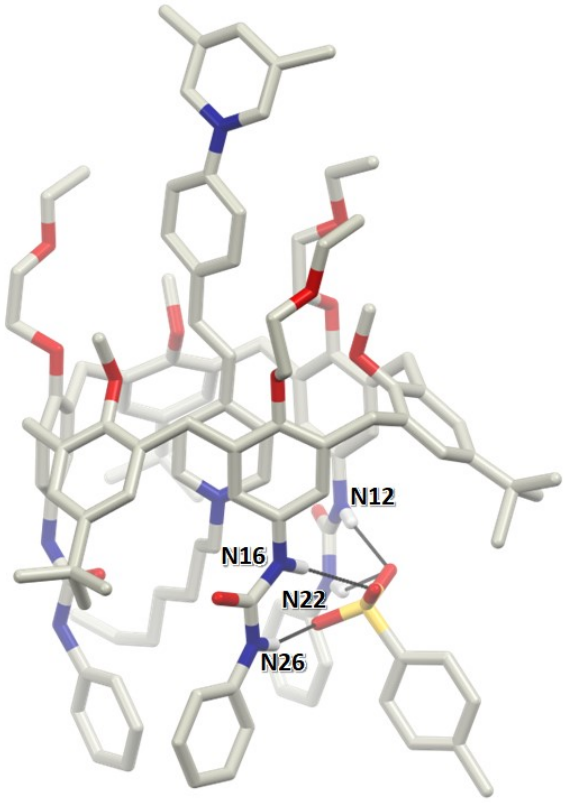

Figure S54. a) X-ray molecular structure of **1-Down** with a partial labelling scheme, showing the hydrogen bond interactions between the N–H groups of phenylureido moieties and the oxygens of tosylate anion (disorder and hydrogen atoms are omitted for clarity).

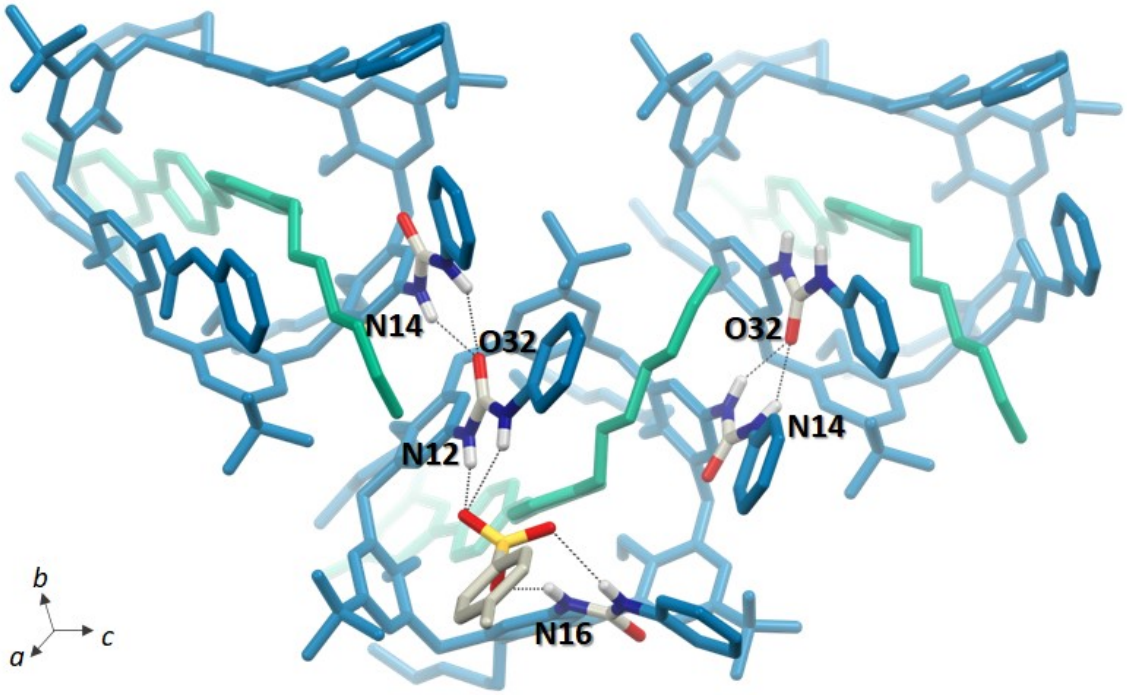

Figure S55. Packing and intermolecular hydrogen bond interactions between neighboring rotaxanes (green colour for stilbazolium guest, light blue colour for the calix[6]arene.

Table S2 Summary of hydrogen bond interactions (Å) for **1-Down**.

NH···OTs interactions			
N12···O1T1	2.93(1)	N16···O1T2	2.97(2)
N16···O3T1	2.96(1)	N26···O3T2	3.12(2)
N26···O3T1	2.86(2)	N12···O2T2	2.94(1)
		N22···O2T2	3.04(1)
NH···O=C interactions			
N14···O32	2.947(5)	N24···O32	3.012(6)

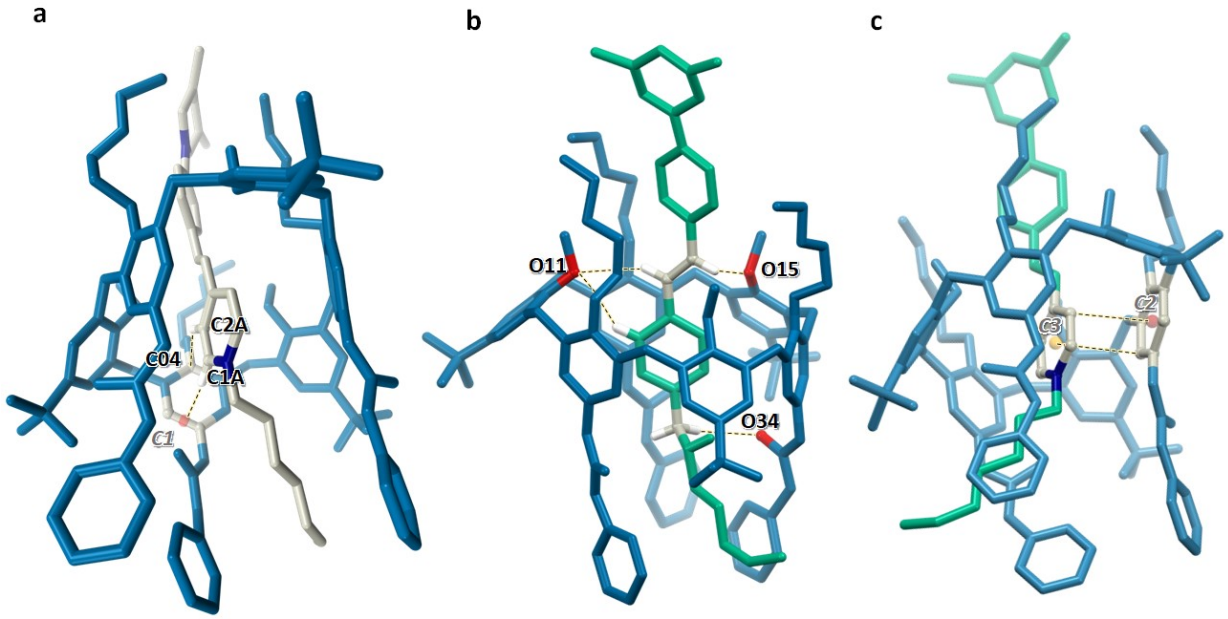

Figure S56. Weak host-guest interactions for **1-Down**: a) CH**---**π, b) CH---O, c) π---π stacking interactions (tosylate anion is omitted for clarity).

Table S3. Selected weak interaction distances (Å) for **1-Down.**

CH···π, and π···π interactions		*CH···O interactions*	
C1S···*Centroid 1*	3.66	C6S···O11	3.473(7)
C2S···C04	3.603(8)	C7S···O15	3.036(6)
C4S···*Centroid 2*	3.295	C7S···O13	3.478(6)
C46···*Centroid 3*	3.416	C20S···O34	3.32(1)

References

[1] J. J. González, R. Ferdani, E. Albertini, J. M. Blasco, A. Arduini, A. Pochini, P. Prados, J. de Mendoza, *Chem. Eur. J.* 2000, **6**, 73–80.
[2] C. G. Hatchard, C. A. Parker, *Proc. R. Soc. London Ser. A*, 1956, **235**, 518–536
[3] K. Stranius, and K. Börjesson, *Sci Rep*, 2017, **7**, 41145.
[4] https://berkeley-madonna.myshopify.com/
[5] C. Feldmeier, H. Bartling, E. Riedle and R. M. Gschwind, *J. Magn. Reason.*, 2013, **232**, 39–44.
[6] *CrysAlis PRO*. Agilent Technologies Ltd, Yarnton, Oxfordshire, England.
[7] G. M. Sheldrick, *Acta Cryst.* 2015, **A71**, 3-8
[8] O. V. Dolomanov, L. J. Bourhis, R. J. Gildea, J. A. K. Howard, and H. Puschmann, *J. Appl. Cryst.,* 2009, **42**, 339.
[9] G. M. Sheldrick, Acta Cryst. 2015, **C71**, 3-8.
[10] D. Osmaniye, B. Kaya Cavusoglu, B. N. Saglik, S. Levent, U. Acar Cevik, O. Atli, Y. Ozkay, and Z. A. Kaplancikli, *Med. Chem. Res.,* 2020, **29**, 1000–1011
[11] H. Görner, *J. Photochem. Photobiol. A Chem.*, 2011, **218**, 199–203
[12] B. Carlotti, G. Consiglio, F. Elisei, C. G. Fortuna, U. Mazzucato and A. Spalletti, *J. Phys. Chem. A*, 2014, **118**, 3580–3592
[13] http://www.hyperquad.co.uk/
[14] E. Fischer, *J. Phys. Chem.*, 1967, **71**, 3704–3706.
[15] J. Jaumot, A. de Juan and R. Tauler, *Chemometr. Intell. Lab. Syst.*, 2015, **140**, 1–12.